

PREPRINT

Author-formatted, not peer-reviewed document posted on 20/05/2025

DOI: <https://doi.org/10.3897/arphapreprints.e159478>

Molecular and morphological insights into the taxonomy and distribution of the Amazonian snake *Erythrolamprus carajasensis* (Cunha, Nascimento & Ávila Pires, 1985) (Serpentes, Xenodontinae)

 Alessandra Guimarães, Hussam El Dine Zaher,  Gisele Lopes Nunes, Ana Lúcia da Costa Prudente

Disclaimer on biological nomenclature and use of preprints

The preprints are preliminary versions of works accessible electronically in advance of publication of the final version. They are not issued for purposes of botanical, mycological or zoological nomenclature and **are not effectively/validly published in the meaning of the Codes**. Therefore, nomenclatural novelties (new names) or other nomenclatural acts (designations of type, choices of priority between names, choices between orthographic variants, or choices of gender of names) **should NOT be posted in preprints**. The following provisions in the Codes of Nomenclature define their status:

International Code of Nomenclature for algae, fungi, and plants (ICNafp)

Article 30.2: "An electronic publication is not effectively published if there is evidence within or associated with the publication that its content is merely preliminary and was, or is to be, replaced by content that the publisher considers final, in which case only the version with that final content is effectively published." In order to be validly published, a nomenclatural novelty must be effectively published (Art. 32.1(a)); in order to take effect, other nomenclatural acts must be effectively published (Art. 7.10, 11.5, 53.5, 61.3, and 62.3).

International Code of Zoological Nomenclature (ICZN)

Article: 21.8.3: "Some works are accessible online in preliminary versions before the publication date of the final version. Such advance electronic access does not advance the date of publication of a work, as preliminary versions are not published (Article 9.9)".

1 **Molecular and morphological insights into the taxonomy and distribution of the**
2 **Amazonian snake *Erythrolamprus carajasensis* (Cunha, Nascimento & Ávila Pires,**
3 **1985) (Serpentes, Xenodontinae)**

4
5 Alessandra Cavalcante Guimarães^{1,2,4}, Hussam Zaher³, Gisele Lopes Nunes⁴, Ana
6 Lúcia da Costa Prudente^{1,2}

7
8 ¹ *Laboratório de Herpetologia, Coordenação de Zoologia, Museu Paraense Emílio*
9 *Goeldi, Avenida Perimetral 1901, 66040-170, Belém, Pará, Brazil.*

10 ² *Programa de Pós-Graduação em Zoologia, Universidade Federal do Pará / Museu*
11 *Paraense Emílio Goeldi, Belém, Pará, Brazil.*

12 ³ *Museu de Zoologia da Universidade de São Paulo, Avenida Nazaré, 04263-000, São*
13 *Paulo, Brazil.*

14 ⁴ *Instituto Tecnológico Vale, Belém, Pará, Brazil.*

15
16 Corresponding author: Alessandra C. Guimarães (alessandraserps@gmail.com)

17
18 **Abstract:** *Erythrolamprus carajasensis* was originally described from the canga areas
19 of the Carajás region in the state of Pará, Brazil, and its distribution is restricted to the
20 type locality. The species exhibits morphological similarities to *E. almadensis*, which
21 has a parapatric distribution. In this study, we investigated the taxonomic status of *E.*
22 *carajasensis* using both molecular and morphological data. We generated mitochondrial
23 gene sequences (12S rRNA and 16S rRNA) for three specimens of *E. carajasensis* and
24 11 specimens of *E. almadensis* and compared them with sequences available in
25 GenBank for Bayesian phylogenetic inference. We examined specimens of *E.*
26 *carajasensis*, including its type series, and compared them with morphologically related
27 and congeneric taxa. Our analysis included meristic and morphometric characters, color
28 patterns, hemipenis and cranial osteology. Our integrative approach thus supports the
29 recognition of *E. carajasensis* as a distinct evolutionary lineage from *E. almadensis*,
30 despite their morphological conservatism in some characters. The skull differences
31 observed, which are congruent with the molecular phylogeny and geographic
32 distribution, justify the redefinition of *E. carajasensis* to include Amazonian
33 populations formerly attributed to *E. almadensis*. In contrast, *E. almadensis* is now
34 restricted to extra-Amazonian populations in Brazil, primarily those occurring in the
35 Atlantic Forest, Cerrado, and ecotonal regions with the Caatinga, in eastern and
36 southern Brazil. The geographic separation between *E. almadensis* and *E. carajasensis*
37 is primarily delineated by the Amazon–Tocantins interfluve, reflecting ecological and
38 possibly historical barriers to dispersal.

39
40
41 **Keywords:** Morphology, Phylogeny, Integrative taxonomy, Xenodontini.

42 Introduction

43

44 *Erythrolamprus* Boie, 1826 represents the most diverse genus within the tribe
45 Xenodontini Bonaparte, 1845, comprising 56 species (Uetz et al. 2024) distributed from
46 Central America and the Trans-Andean region to northwestern Argentina (Peters and
47 Orejas-Miranda 1970; Dixon 1980; Dixon 1989; Grazziotin et al. 2012). The
48 monophyly of *Erythrolamprus* has been supported by several molecular studies (Zaher
49 et al. 2009, 2019; Vidal et al. 2010; Grazziotin et al. 2012; Pyron et al. 2013; Figueroa
50 et al. 2016; Murphy et al. 2019; Torres-Carvajal and Hinojosa 2020, 2024), although no
51 morphological autapomorphy has yet been identified for the genus (Myers 1986; Zaher
52 et al. 2009; Grazziotin et al. 2012). Furthermore, the interspecific relationships within
53 the genus remain poorly resolved (Torres-Carvajal and Hinojosa 2020, 2024; Serrano et
54 al. 2024), and many described taxa have yet to be placed in a phylogenetic context.

55

56 Most *Erythrolamprus* species are defined by their morphological characters,
57 mainly related to their coloration patterns (Dixon 1983a, b, 1987, 1991; Dixon and
58 Thomas 1985; Dixon and Markezich 1992; Ascenso et al. 2019). However, many
59 species exhibit color polymorphism (Dixon and Markezich 1992; Ascenso et al. 2019;
60 Hudson et al. 2021), and some color patterns have evolved several times independently
61 in different lineages (Murphy et al. 2019). The presence of extensive color
62 polymorphisms within populations that otherwise exhibit uniform morphology across
63 other anatomical features complicates the identification and delimitation of taxa within
64 this genus (Murphy et al. 2019).

65

66 *Erythrolamprus carajasensis* (Cunha, Nascimento & Ávila-Pires, 1985) was
67 described based on external morphology from a series of 28 specimens collected
68 exclusively in the canga areas of Serra Norte, Carajás region, State of Pará, Brazil.
69 Dixon (1991) noted a similarity in coloration between *E. carajasensis* and *E.*
70 *almadensis* (Wagler, 1824), mainly due to a light parietal mark. However, hesitated to
71 synonymize the species due to observed differences in the number of subcaudal scales.
72 The distribution of *E. almadensis* is parapatric with that of *E. carajasensis*, with
73 marginal records in the Amazon. *E. almadensis* is known to inhabit several plant
74 formations in Brazil, occurring in the Caatinga, Cerrado, Pantanal, Pampas, and Atlantic
75 Forest, as well as in the Chacos of Bolivia, Argentina, Uruguay, and Paraguay (Dixon
76 1991; Nogueira et al. 2019).

77

78 *Erythrolamprus carajasensis* is considered an endemic species facing ongoing
79 threats within its distribution area and is categorized as Data Deficient (DD) in the
80 IUCN (Silveira et al. 2021). In this study, we integrated multiple sets of evolutionary
81 evidence and employed extensive sampling, in order to elucidate the taxonomic status
82 of *E. carajasensis*. We analyzed genetic and morphological data, including meristic and
83 morphometric characters, color patterns, as well as hemipenis and cranial osteology.

84

85 Materials and Methods

86

87 Molecular analysis

88

89 We generated sequences for the mitochondrial 12S rRNA and 16S rRNA genes for
 90 three specimens of *Erythrolamprus carajasensis* and 11 specimens of *E. almadensis*
 91 (Table 1).

92
 93
 94

Table 1. Vouchers, locality data, and GenBank accession numbers of the specimens and gene regions included in this study.

Taxon	Voucher	Locality	12S	16S
<i>E. almadensis</i>	IBSP 80677	Brazil: Tocantins	PP739075	PP736061
<i>E. almadensis</i>	IBSP 80887	Brazil: São Paulo, Jambeiro	PP739076	PP736062
<i>E. almadensis</i>	IBSP 92040	Brazil: Minas Gerais, São Roque de Minas	PP739077	PP736063
<i>E. almadensis</i>	IBSP 92154	Brazil: São Paulo, Araçariguama	PP739078	PP736064
<i>E. almadensis</i>	IBSP 92720	Brazil: Santa Catarina, Lages	PP739079	PP736065
<i>E. almadensis</i>	MCP 19055	Brazil: Rio Grande do Sul, Viamão	PP739081	PP736067
<i>E. almadensis</i>	TR 972	Brazil: Bahia, Salvador	PP739087	PP736073
<i>E. almadensis</i>	TR 995	Brazil: Bahia, Salvador	PP739088	PP736074
<i>E. almadensis</i>	TR 437	Brazil: Bahia, Salvador	PP739086	PP736072
<i>E. almadensis</i>	MPEG 21966	Brazil: Mato Grosso, Querência	PP739085	PP736071
<i>E. almadensis</i>	INPAH 39310	Brazil: Amazonas, Canutama	PP739080	PP736066
<i>E. carajasensis</i>	MPEG 27436	Brazil: Pará, Canaã dos Carajás	PP739082	PP736068
<i>E. carajasensis</i>	MPEG 27437	Brazil: Pará, Canaã dos Carajás	PP739083	PP736069
<i>E. carajasensis</i>	MPEG 26722	Brazil: Pará, Canaã dos Carajás	PP739084	PP736070

95
 96
 97
 98
 99
 100
 101
 102

We extracted total DNA from the liver, muscle and scales using the DNeasy Blood and Tissue Kit (Qiagen) and quantified it with a Qubit fluorometer (Thermo Fisher Scientific), following the manufacturers' protocols. We then amplified fragments of the 12S and 16S rRNA mitochondrial genes via polymerase chain reaction (PCR) using the primers L1091mod and H1557mod for 12S and L2510mod and H3056mod for 16S, as described by Zaher et al. (2009). We performed the PCR using PCR Master Mix (Promega), following the protocols described by Graziotin et al. (2012). We

103 enzymatically purified the amplification products using ExoSap-IT and sequenced then
104 on a SeqStudio® (Thermo Fisher Scientific®) platform, according to the manufacturer's
105 protocols, at the Molecular Biology Laboratory of the Museu Paraense Emílio Goeldi
106 (MPEG).

107
108 We assessed the quality of the chromatograms and generated consensus
109 sequences using Geneious® 7.1.3 (Kearse et al. 2012). Subsequently, we aligned the
110 sequences using MAFFT version 7.526 (Kato et al. 2019), applying the Q-INS-I
111 algorithm and default parameters for gap opening and extension. After alignment, we
112 concatenated the datasets using Sequence Matrix 1.8 software (Vaidya et al. 2011). To
113 select partitioning schemes and models of molecular evolution, we used IQ-TREE 2
114 (Minh et al. 2020), applying the Akaike Information Criteria (AIC). We inferred
115 phylogenetic relationships among taxa using the Bayesian Inference (BI) with MrBayes
116 implemented via the CIPRES online portal (Miller et al. 2010). We reconstructed the
117 phylogeny using two simultaneous runs with four Markov chains each. Each run
118 consisted of 20 million generations, with sampling every 2,000 generations, and we
119 discarded the first 25% of the trees as burn-in. We assessed parameters convergence for
120 each run using Tracer v.1.7 (Rambaut et al. 2018). Additionally, we calculated
121 uncorrected genetic distance using 16S rRNA fragments in MEGA (Kumar et al. 2016).

122
123 We compared all sequences generated in this study with those available in
124 GenBank for *Erythrolamprus* and the selected outgroup (Supplementary Material 1).
125 We rooted the phylogeny with *Dipsas catesbyi* (Sentzen, 1796) and including *Lygophis*
126 Fitzinger, 1843, *Xenodon* Boie, 1826, *Eutrachelophis papilio* Zaher & Prudente, 2019
127 and *Arcanumophis problematicus* (Myers, 1986) as outgroups. We selected these taxa
128 based on previous phylogenetic hypotheses for Xenodontinae (Figueroa et al. 2016;
129 Grazziotin et al. 2012; Pyron et al. 2013; Zaher et al. 2019; Moraes et al. 2021; Serrano
130 et al. 2024).

131
132 *Morphological analysis*

133
134 We examined a total of 342 specimens, including 70 specimens of
135 *Erythrolamprus carajasensis*, of which 28 comprised the type series. Additionally, we
136 examined comparative material of *E. almadensis* (n = 235) and other congeners from
137 the Amazon region, as follows: *E. poecilogyrus* (Wied-Neuwied, 1825) (n = 22); *E.*
138 *aenigma* Entiauspe-Neto, Abegg, Koch, Nuñez, Azevedo, Moraes, Tiutenko, Bialves &
139 Loebmann, 2021 (n = 4); *E. typhlus* (Linnaeus, 1758) (n = 2); *E. oligolepis* (Boulenger,
140 1905) (n = 2); *E. miliaris* (Linnaeus, 1758) (n = 1); *E. rochai* Ascenso, Costa &
141 Prudente, 2019 (n = 1); *E. reginae* (Linnaeus, 1758) (n = 1); *E. breviceps* (Cope, 1860)
142 (n = 1); *E. taeniogaster* (Jan, 1863) (n = 1); *E. viridis* (Günther, 1862) (n = 1); and *E.*
143 *aesculapii* (Linnaeus, 1758) (n = 1) (Supplementary Material 2). These specimens are
144 housed in the herpetological collections of the following institutions: Coleção Zoológica
145 da Universidade Federal do Mato Grosso do Sul (ZUFMS); Instituto Nacional de
146 Pesquisas da Amazônia (INPA); Museu de Ciências e Tecnologia da Pontifícia
147 Universidade Católica do Rio Grande do Sul (MCP); Museu Nacional do Rio de
148 Janeiro (MNRJ); Museu Paraense Emílio Goeldi (MPEG); Museu de Zoologia da
149 Universidade Federal da Bahia (MZUFBA); Museu de Zoologia da Universidade de

150 São Paulo (**MZUSP**); and Coleção Herpetológica da Universidade de Brasília
151 (**CHUNB**).

152

153 We also used meristic data and measurements of snout-vent length (**SVL**) and
154 caudal length (**CL**), collected by H. Zaher from 191 specimens of *Erythrolamprus*
155 *almadensis*, which were unfortunately lost in the fire that destroyed most of the
156 herpetological collection of the Butantan Institute (**IBSP**) in May 2010 (Kumar 2010;
157 Warrell et al. 2010; Franco 2012). We based our analysis of the *E. almadensis* type
158 specimen (ZSM 2688/0; lectotype of *Natrix almada*) on digital photographs and
159 illustrations (Wagler 1824; Jan and Sordelli 1866), as well as on information from the
160 original descriptions (Wagler 1824) and subsequent taxonomic revisions (Hoogmoed
161 and Gruber 1983; Dixon 1991).

162

163 We determined sexual maturity by analyzing gonadal development, considering
164 adults those individuals with an SVL equal to or greater than of the smallest
165 reproductive individual ($SVL \geq 29$ cm). We verified sex by checking for the presence or
166 absence of a hemipenis through a ventral incision at the base of the tail. We prepared
167 preserved hemipenes following the techniques of Zaher and Prudente (2003) and used
168 the terminology for hemipenial structures established by Zaher (1999). To describe the
169 color pattern, we examined preserved specimens from scientific collections and
170 photographs of live specimens. We evaluated the color pattern of the head, body, and
171 tail in the dorsal, lateral and ventral views based on the criteria described by Dixon
172 (1989, 1991) and Ascenso et al. (2019). We followed the terminology for cephalic
173 shields proposed by Peters (1964) and adopted the ventral and subcaudal counts method
174 of Dowling (1951). We collected the following meristic data: supralabials (**SL**);
175 supralabials in contact with the orbit (**SLo**); infralabials (**IL**); infralabials in contact
176 with anterior chinshields (**IL-Ma**); dorsal scales (anterior, middle, and posterior) of the
177 body (**DO**); ventrals (**VE**); and subcaudals (**SC**). We also recorded morphometric data
178 from the cephalic region, including head length (**HL**), height (**HH**), and width (**HW**);
179 frontal length (**FL**) and width (**FW**); parietal length (**PL**) and width (**PW**); pre-frontal
180 length (**PFL**) and width (**PFW**); internasal length (**INL**) and width (**INW**); orbit
181 diameter (**OD**); orbit-rostral distance (**ORD**); loreal height (**LoH**) and length (**LoL**);
182 anterior (**ACL**) and posterior chinshields length (**PCL**); and rostral height (**RH**) and
183 width (**RW**). We took all measurements using a digital caliper (0.1 mm), while we
184 measured snout-vent length (**SVL**) and caudal length (**CL**) with a flexible ruler (1.0
185 mm).

186

187 To describe cranial osteology, we generated X-ray computed tomography (μ CT)
188 images for specimens of *E. carajasensis* and *E. almadensis* (Supplementary Material 2).
189 We also used μ CT images available on MorphoSource for an *E. almadensis* ([UMMZ](#)
190 [204158](#)) housed at the Museum of Zoology (**UMMZ**), Michigan, USA. We conducted
191 CT scans using a GE Phoenix v|tome|x M 240 system (GE Sensing and Inspection
192 Technologies GmbH, Germany) at the Laboratório de Microtomografia of the Museu
193 Paraense Emílio Goeldi, Pará, Brazil, and a GE Phoenix v|tome|x M 300 (General
194 Electric Measurement & Control Solutions, Wunstorf, Germany) at the Laboratório de
195 Microtomografia of the Museu de Zoologia, Universidade de São Paulo. For each
196 individual specimen, we set specific scan parameters, including exposure time (ms),
197 number of projections, kilovoltage (kV), and current strength (μ A). Scan duration

198 varied depending on the selected configuration. We reconstructed the raster images
199 using Phoenix data|x software and imported then into VG Studio Max 3.4.2 software
200 (Volume Graphics GmbH, Heidelberg, Germany). We followed the osteological
201 terminology proposed by Cundall and Irish (2008) and Zaher et al. (2023).

202

203 We tested the meristic and morphometric characters among the lineages
204 recovered in our molecular phylogenetic analysis using R version 4.2.0 (R Core Team
205 2022). We generated graphical representations using the *ggplot2* package (Wickham
206 2016). We assessed statistical significance at 5% and presented descriptive statistics as
207 means \pm standard deviations (SD). We tested the data for normality and
208 homoscedasticity of variances using the Shapiro–Wilk and Levene tests, respectively.

209

210 To minimize allometric effects, we included only adults in the morphometric
211 analysis and size-corrected the data by SVL using the allometric formula of Thorpe
212 (1975) for multispecies datasets, implemented in the R package *GroupStruct* (Chan and
213 Grismer 2022). We used the Wilcoxon test to evaluate sexual dimorphism and
214 determine whether the means of morphological characters differ significantly among
215 lineages. We performed a Principal Component Analysis (PCA) to visualize and assess
216 the degree of morphospacial clustering, using the 'nipals' function from the R package
217 *pcaMethods*. We also conducted Discriminative Principal Component Analysis (DPCA)
218 (Jombart and Collins 2015) using the R package *adeget* to evaluate the distinction
219 between predefined groups.

220

221 We obtained geographic coordinates for samples from original field records and
222 literature sources. For locations without available coordinates, we georeferenced them
223 using Google Earth Pro software (Google Earth Pro 2022). We standardized the
224 coordinates to decimal degrees by converting them to the SIRGAS 2000 datum and
225 constructed maps using QGIS 3.24 software (QGIS 2023).

226

227 **Results**

228

229 *Phylogenetic analyses*

230

231 Our concatenated alignment consisted of 1,167 base pairs (bp), with 521 bp for the 12S
232 rRNA gene and 646 bp for the 16S rRNA gene. The concatenated alignment had a gap
233 and undetermined characters proportion of 43.63%. The best partitioning scheme and
234 the best-fitting model selected for the 12S and 16S ribosomal fragments were
235 GTR+F+I+G4. The consensus tree generated by Bayesian Inference (Fig. 1,
236 Supplementary Material 3) strongly supported the monophyly of Xenodontini with high
237 support values (PP = 0.99). Within Xenodontini, *Xenodon* was recovered as the sister
238 clade of *Erythrolamprus*.

239

240 The genus *Erythrolamprus* was recovered as paraphyletic, with *E. sagittifer*
241 closely related to the clade containing *Lygophis anomalus* (Günther, 1858) and *Ly.*
242 *elegantissimus* (Koslowsky, 1896), with maximum support (PP = 1). The remaining
243 *Erythrolamprus* species formed a strongly supported clade (PP = 1), which consisted of
244 two main clades: clade A, with low support (PP = 0.89), formed by *E. atraventer*
245 (Dixon & Thomas, 1985) as a sister group of the clade containing *E. jaegeri* (Gunter,

246 1858), *E. almadensis* and *E. carajasensis*; and clade B, which included all other species
247 of the genus, with relatively low support (PP = 0.46) (Fig. 1).

248

249 In clade A, *Erythrolamprus almadensis* was recovered with maximum support
250 (PP = 1), and it contained two subclades: subclade A1 (PP = 1), which included *E.*
251 *carajasensis* nested among specimens from the states of Amazonas and Mato Grosso;
252 and subclade A2 (PP = 0.94), which consisted of specimens from Bahia, Tocantins,
253 Minas Gerais, São Paulo, and specimens from the southern part of the distribution,
254 including Rio Grande do Sul and Santa Catarina (Fig. 1).

255

256 The uncorrected genetic distances based on the mitochondrial 16S rRNA gene
257 among the *Erythrolamprus* species ranged from 0.00 to 0.10 (0.035±0.017). The
258 smallest distances were observed between *E. ceii* and *E. poecilogyrus*, while the largest
259 distances were observed between *E. sagittifer* and *E. mimus* (Cope, 1868). *E.*
260 *carajasensis* presented the smallest genetic distances with *E. almadensis*, ranging from
261 0.002 to 0.004 for specimens from subclade A1 (Amazonia), and from 0.011 (Salvador,
262 Bahia, approximately 200 km from the type locality of *E. almadensis*) to 0.018
263 (southern Brazil) for specimens from subclade A2 (Supplementary Material 4).

264



Figure 1. Bayesian inference tree of phylogenetic relationships in Xenodontini based on the 12S and 16S rRNA mitochondrial genes. The numbers next to the branches are the Supporting Posterior Probability (PP) values.

265

266 *Morphological analyses*

267

268

269

270

271

272

273

274

275

276

We observed overlapping morphological characters among the recovered lineages (Table 2). The Wilcoxon test revealed significant differences ($p < 0.05$) in morphometric characters between males and females of the subclades A1 (SVL, HL, HW, HH, FL, PL, INW, ORD, ACL, PCL, RW, and RH) and A2 (SVL, CL, and ACL), with females being larger than males. Therefore, we treated the sexes separately in subsequent statistical analyses.

Table 2. Descriptive statistics of external morphological characters between specimens of subclades A1 and A2.

Characters / Taxon	Subclade A1		Subclade A2	
	Females	Males	Females	Males
Number of specimens	73	43	213	168
Ventrals range	146–168	151–161	145–170	140–166
Mean ventrals \pm SD	155 \pm 3.3	155 \pm 2.4	155 \pm 4.06	155 \pm 3.8
Subcaudals range	54–77	49–75	54–78	57–76
Mean subcaudals \pm SD	64 \pm 5.6	66 \pm 5.8	64 \pm 3.6	64 \pm 3.5
SVL range	12.4–47.6	13.1–38.9	12.3–50.5	13.8–42.8
Mean SVL \pm SD	28.8 \pm 9.2	26.6 \pm 7.13	34.1 \pm 8.4	30.9 \pm 6.1
CL range	3.2–13.1	4.2–11.4	3.5–14.8	3.8–12.3
Mean CL \pm SD	8.39 \pm 2.51	8.26 \pm 2.17	9.9 \pm 2.4	9.3 \pm 1.98

277

278

279

280

281

282

283

284

285

286

287

288

289

290

291

Analyzing subclades A1 and A2 of *Erythrolamprus almadensis*, we observed significant differences ($p < 0.05$) in the morphometric characters. Females differed in CL, HL, HW, HH, FL, FW, PW, ORD, ACL, RW and RH, while males showed differences in HW, HH, FW, ACL, RW, and RH. The first two axes of the PCA explained 42.05% of the total variation for females (PC1 = 28.05%; PC2 = 14.00%) and 42.42% for males (PC1 = 26.19%; PC2 = 16.23%) among subclades A1 and A2 (Figs. 2A and 2B). The characters SC and LoL contributed most to the formation of the first and second axes, respectively. PCA results showed an overlap of morphological characters between the subclades. The DAPC results successfully discriminate between the two groups based on external morphology. For females, the first linear discriminant explained 99.28% of the total variance, with 95.91% of the specimens correctly assigned to their subclades. For males, the first linear discriminant explained 99.28% of the variance, with 91.48% of the specimens correctly assigned (Figs. 2C and 2D).

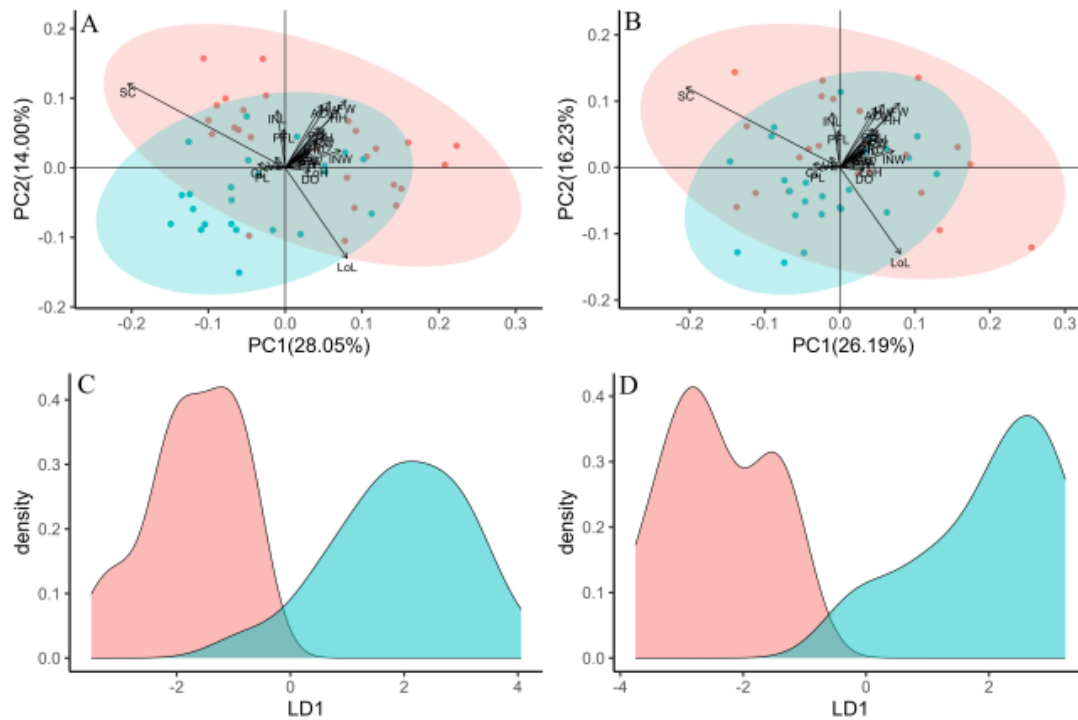


Figure 2. Graphical representations of the variation explained by the principal component analysis (PCA) (A, B) and the discriminative principal component analysis (DPCA) (C, D) for the comparison of meristic and morphometric characters. The graphs on the left show the variation for females, and those on the right show the variation for males. Legend: subclade A1 (red) and subclade A2 (blue).

292
 293
 294
 295
 296
 297
 298
 299
 300
 301
 302
 303
 304
 305
 306
 307
 308

We observed that *Erythrolamprus carajasensis* and *E. almadensis* share many similarities in coloration pattern, as follows: **Head** – gray, dark gray or brown dorsal region, with a light mark (ranging from white to cream) usually in a “V” or “Y” shape, formed by the inner edges of the parietal scales; lateral region with irregular dark dots (ranging from brown, dark gray to black) between the supralabials; ventral region with small irregular dark spots or dots (ranging from dark gray to black) present on the gular scales; **Body** – gray, dark gray or brown dorsal region, with dark dorsal bands (ranging from dark gray to black or brown) that become irregular blotches in the midbody; light dorsolateral stripe along the body, between scales rows 5 and 6 in *E. carajasensis*, and between scales 5 and 6 or 5 and 7 in *E. almadensis*; cream belly with black bands at the lateral extremities of the ventrals; and **Tail** – dorsal region varying from gray to dark gray; ventral region cream, rarely with irregular spots (Fig. 3). Adult specimens of subclade A1 usually exhibit dorsal coloration that is gray or dark gray, with melanic patterns being very common, while lighter color patterns are often observed in juveniles.

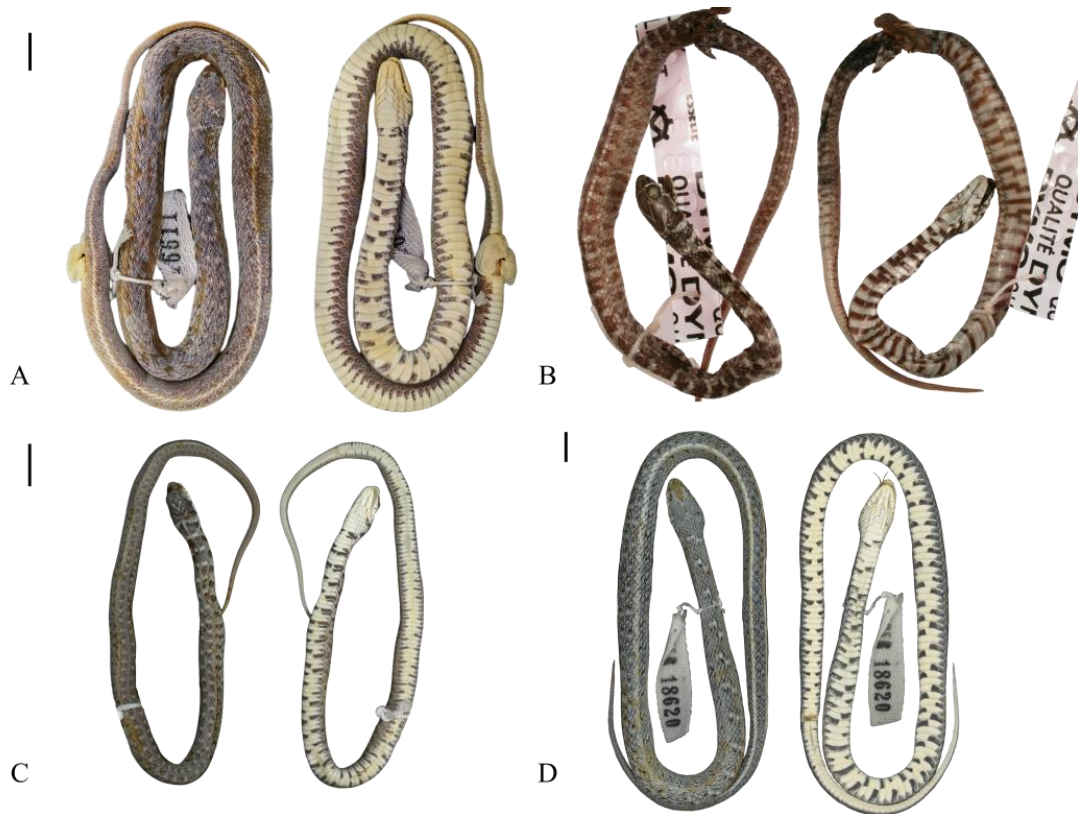


Figure 3. Dorsal (left) and ventral (right) views of the **A** holotype of *Liophis carajasensis* (MPEG 16611, adult), **B** lectotype of *Natrix almadensis* (ZSM 2688/0, juvenile), **C** topotype of *Erythrolamprus carajasensis* (MPEG 17142, juvenile) and **D** *E. almadensis* from Feira de Santana, Bahia, Brazil (MPEG 18620, adult). Scale bar: 1 cm.

309

310

311 The hemipenes of *Erythrolamprus carajasensis* and *E. almadensis* were found to

312 be nearly identical. Notable similarities include the shape of the organ, the presence of a

313 nude region at the base of the lobes on the asulcate face; the shape and size of the lateral

314 prominences ornamented with enlarged spines on the proximal region on the asulcate

315 face of body; the medial region ornamented with row of slightly enlarged spinules on

316 the asulcate surface of the body; and the intrasulcal region with spinules distributed

317 homogeneously (Fig. 4). Some specimens exhibit variation in the morphology of the

318 lateral spines, which may appear more robust and arranged in fewer rows, or

319 alternatively, slender and arranged in a greater number of rows; and as to the row of

320 distinctly enlarged spinules on the asulcate surface. These variations are present in

321 specimens throughout the distribution of *E. almadensis* and *E. carajasensis*, and within

322 the lineages recovered.

322

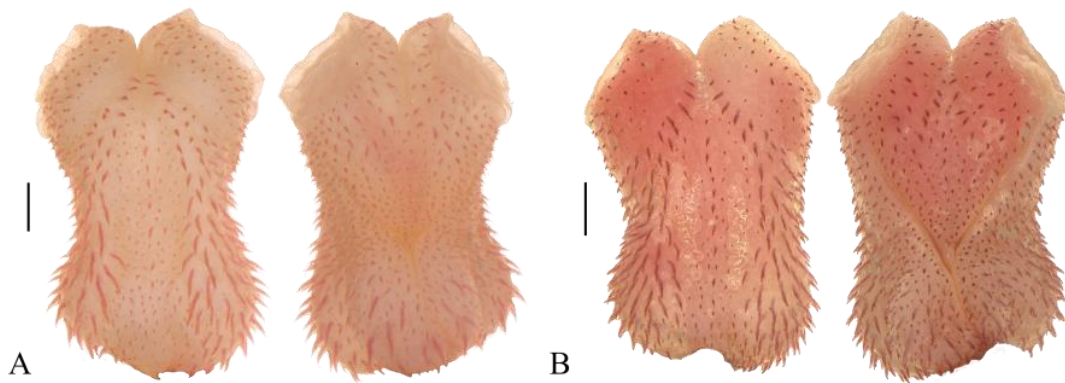


Figure 4. Asulcate (left) and sulcate views of the hemipenis of **A.** *Erythrolamprus carajasensis* from Parauapebas, Pará, Brazil (MPEG 24478) and **B** *E. almadensis* from Salvador, Bahia, Brazil (UFBA 373). Scale bar = 2 mm.

323

324

325

326

327

328

329

330

331

332

333

334

335

336

337

338

339

340

341

342

343

344

345

346

347

348

349

350

351

352

353

354

355

356

357

The general shape and position of the skull structures, as well as the number of teeth and the position of the foramina, are similar between *Erythrolamprus carajasensis* and *E. almadensis*, as well as among specimens from subclades A1 and A2 (Fig. 5; Table 3). We observed small intraspecific and interspecific variations in the tip of the palatine process of the vomer, which may be blunt or tapering, the supratemporal which may be arched or straight, and in the lateral process of the prefrontal, which can be shorter or more pronounced in some specimens.

Additionally, specimens from the Carajás region exhibit more slender cranial bone structures compared to other specimens of subclade A1 and A2. These differences include: a quadrate that is slender and straight with a reduced posterior edge, being robust and obliquely inclined in other specimens; an articular process of the compound bone that is slender and more dorsally prominent; a narrower ascending lateral lamina of the septomaxilla; a shorter dorsal lateral lamina of the nasal; and a generally shorter quadrate process of the pterygoid (Table 3).

However, in subclade A1 the supratemporal is arched in dorsal view, the prearticular crest of the adductor fossa is well developed, and the surangular crest is reduced and directed dorsolaterally. In contrast, in subclade A2, the supratemporal is straight in dorsal view, and both the articular and surangular crests are well developed, with adductor fossa dorsally directed; the quadrate has a broader cephalic end, occupying more than half the length of the supratemporal; the mandibular foramen is oriented laterally in subclade A1, but may be dorsolaterally in subclade A2; and the ascending process of the premaxilla appears tapered in dorsal view in subclade A1 but possibly blunt in subclade A2 (Table 3).

Despite the overlap in meristic and morphometric characters, as well as similarities in coloration patterns and hemipenial morphology, the lineages recovered in the molecular phylogeny can be distinguished by skull morphology. We redefine *Erythrolamprus carajasensis* to include the Amazonian populations previously identified as *E. almadensis* (subclade A1) and restrict *E. almadensis* to the extra-Amazonian populations (subclade A2). We present redescrptions of both species based on a larger sample size that encompasses the observed morphological variation and provide updated maps of their current geographic distributions.

358

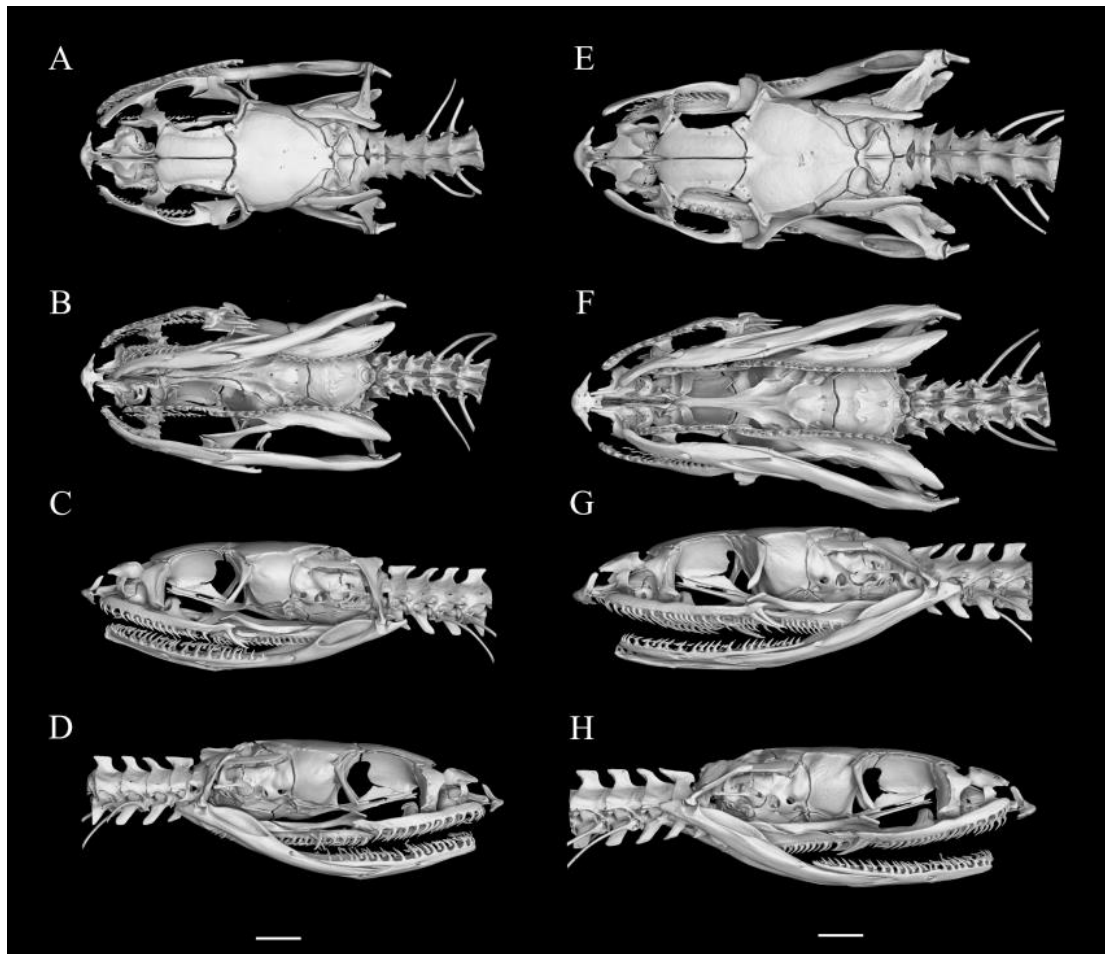


Figure 5. Skulls of *Erythrolamprus carajasensis* from Parauapebas Pará, Brazil (MPEG 17000) **A, D** and of *E. almadensis* from Feira de Santana, Bahia, Brazil (MPEG 18620) **E, H**; dorsal, **A** and **E**; ventral **B** and **F**; left lateral **C** and **G**; right lateral, **D** and **H**. Scale bar = 2 mm.

359
360
361

Table 3. Comparison of cranial osteological characters of *Erythrolamprus carajasensis* and *E. almadensis* based on X-ray computed tomography (μ CT).

Osteological characters	<i>E. carajasensis</i> (subclade A1)	<i>E. almadensis</i> (subclade A1)	<i>E. almadensis</i> (subclade A2)
PrediaSTEMal tooth count	20–22	19–21	19–22
Palatine tooth count	15	14–16	16
Pterygoid tooth count	28–31	25–28	27–30
Dentary tooth count	28–29	29–30	28–30
Quadrates	Slender and straight	Robust and obliquely sloping	Robust and obliquely sloping
Lateral lamina of the septomaxilla	Narrow	Wide	Wide

Lateral lamina of the nasal	Shorter	Longer	Longer
Quadrate process of the pterygoid	Short	Long	Long
Position of the surangular crest	Laterally	Laterally	Dorsolaterally
Orientation of the mandibular foramen	Laterally	Laterally	Laterally or dorsolaterally
Dorsal view of the ascending process of the premaxilla	Tapered	Tapered	Tapered or blunt

362

363

Taxonomy

364

365

***Erythrolamprus carajasensis* (Cunha, Nascimento e Ávila-Pires, 1985)**

366

367

Liophis carajasensis Cunha, Nascimento and Ávila-Pires 1985: 53. Type locality: Serra

368

Norte, Carajás, Pará, Brazil. Holotype: MPEG 16611 (Fig. 3A); Wallach et al.

369

2014: 388.

370

Erythrolamprus carajasensis — Grazziotin et al. 2012; Nogueira et al. 2019.

371

372

Holotype: Adult male, MPEG 16611, collected by the Goeldi Museum team on

373

November 18, 1983, in a rocky field in the Serra Norte, Carajás region, municipality of

374

Parauapebas, Pará state, Brazil (6°01'50.0"S 50°17'15.0"W) (Fig. 3A). Erroneously

375

listed also as a paratype by Cunha et al. (1985).

376

377

Paratypes: Twenty-seven specimens, all from the Serra Norte rupestrian field, Carajás

378

region, municipality of Parauapebas, Pará state, Brazil: juvenile female, MPEG 81;

379

collected in May 1969; juvenile female, MPEG 16500; juvenile male, MPEG 16501;

380

juvenile male, MPEG 16503; juvenile female, MPEG 16505; adult male, MPEG 16506;

381

juvenile female, MPEG 16507; juvenile female, MPEG 16508; juvenile female, MPEG

382

16509; juvenile female, MPEG 16510; juvenile male, MPEG 16511; juvenile female,

383

MPEG 16512; juvenile female, MPEG 16513; juvenile female, MPEG 16516; juvenile

384

male, MPEG 16519 (erroneously considered female in the original description);

385

juvenile male, MPEG 16520; collected in May 1983; juvenile female, MPEG 16522;

386

juvenile female, MPEG 16529; juvenile male, MPEG 16545; juvenile female, MPEG

387

16591; adult female, MPEG 16598; adult male, MPEG 16600; adult male, MPEG

388

16606; adult female, MPEG 16613; adult female, MPEG 16617; adult female, MPEG

389

16771; adult female, MPEG 16790.

390

391

Diagnosis. *Erythrolamprus carajasensis* is distinguished from all its congeners by the

392

unique combination of the following characters: (1) 19 rows of dorsal scales, reducing

393 to 17 rows after the midbody; (2) single preocular; (3) ventrals 146–168; (4) subcaudals
 394 49–77; (5) SVL 124–476 mm in females and 131–389 in males; (6) CL 32–131 mm in
 395 females and 42–114 in males; (7) single apical pit; (8) dorsal region of the head with a
 396 light mark formed by the inner edges of the parietals; (9) light dorsolateral stripes,
 397 extending from the anterior region to the tail, between scale rows 5 and 6; (10) cream
 398 belly in preserved material, red in life, with black bands; (11) absence of spines in the
 399 median region of the asulcate face of the hemipenis; (12) well-developed prearticular
 400 crest of the adductor fossa, and reduced surangular crest directed dorsolaterally; and
 401 (13) supratemporal arched in dorsal view.

402

403 **Comparisons:** *Erythrolamprus carajasensis* differs from congeners with 19/19/17
 404 dorsal scale rows as follows: from *E. almadensis* by reduced surangular crest (vs. well-
 405 developed surangular crest), and arched supratemporal in dorsal view (vs. straight
 406 supratemporal); from *E. atraventer* by gray dorsal coloration, cream belly with black
 407 bands, and the presence of an apical pit (vs. green dorsal coloration, black belly, and
 408 absence of apical pit); from *E. festae* by having a single preocular (vs. two preoculars);
 409 from *E. taeniurus* (Tschudi, 1845) by the presence of a light dorsolateral stripe (vs.
 410 black lateral stripes bordered by yellow stripes); from *E. viridis* by gray dorsal
 411 coloration and banded belly (vs. uniformly green or green back with black bands and a
 412 uniformly white belly); and from *E. maryellenae* by the presence of an apical pit (vs. the
 413 absence of the apical pit). Differs from *E. aenigma*, *E. ceii* (Dixon, 1991), *E.*
 414 *poecilogyrus* and *E. typhlus* by having 19 dorsal scale rows reducing to 17 at midbody
 415 (vs. reduction to 15); from *E. andinus* (Dixon, 1983), *E. oligolepis* and *E. aesculapii* by
 416 presenting 19 dorsal scale rows at midbody (vs. 15 dorsal scale rows); and from *E.*
 417 *breviceps*, *E. cobella* (Linnaeus, 1758), *E. dorsocorallinus* (Esqueda, Natera, La Marca
 418 & Ilija-Fistar, 2007), *E. frenatus* (Werner, 1909), *E. jaegeri*, *E. macrosomus* (Amaral,
 419 1935), *E. miliaris*, *E. mossoroensis* (Hoge & Lima-Verde, 1973), *E. pygmaeus* (Cope,
 420 1868), *E. reginae*, *E. rochai*, *E. taeniogaster*, *E. trebbai* (Roze, 1958), and *E.*
 421 *semiaureus* (Cope, 1862) by having 19 dorsal scale rows at midbody (vs. 17 dorsal scale
 422 rows).

423

424 **Morphometric and meristic variation** (n = 118). Snout-vent length 124–476 mm in
 425 females (288.4±92.6; n = 73), 131–389 mm in males (266.1±71.32; n = 43); caudal
 426 length 32–131 mm in females (83.9±25.1; n = 72), 42–114 mm in males (82.6±21.7; n =
 427 40); head length 9.5–21.7 mm (14.4 ± 3.2; n = 97), height 3.13–7.7 mm (5.1 ± 1.28; n =
 428 10197), and width 4.4–11.04 mm (6.97 ± 1.67; n = 97); diameter of ocular orbit 1.8–3.5
 429 mm (2.67±0.3; n = 105); distance between the orbit and rostral shield 2.6–6.3 mm
 430 (4.3±0.9; n = 106); rostral triangle, 0.7–1.7 mm high (1.1±0.2; n = 103), 1.6–3.7 mm
 431 wide (2.5±0.5; n = 105); two internals, 0.6–1.6 mm long (1.04±0.2; n = 106), 0.9–2.06
 432 mm wide (1.4±0.2; n = 106); prefrontals 0.8–2.3 mm long (1.5±0.3; n = 106), 0.7–2.7
 433 mm wide (2.503±0.4; n = 106); pentagonal frontal, 3.01–5.3 mm long (4.3±0.5; n =
 434 105), 1.6–3.4 mm wide (2.4±0.4; n = 106); two parietals, 2.2–4.3 mm long (3.2±0.4; n =
 435 105), 2.2–4.1 mm wide (3.2±0.4; n = 106); loreal 0.4–1.4 mm long (0.8±0.2; n = 106),
 436 0.7–1.6 mm high (1.2±0.2; n = 110); anterior chinshields 2.1–4.8 mm long (3.3±0.7; n =
 437 107); posterior chinshields 1.8–4.7 mm long (3.1±0.7; n = 107); ventrals 146–168 in
 438 females (155±3.3; n = 73), 151–161 in males (155± 2.4; n = 39); subcaudals 54–77 in
 439 females (64±5.6; n = 70), 49–75 in males (66±5.8; n = 40); supralabials 8/8 (n = 105),
 440 7/8 (n = 1), 6/7 (n = 1), 4th and 5th in contact with the orbit; infralabials 10/10 (n = 86),

441 9/10 (n = 16), 8/10 (n = 3), with 4 (n = 82), 5 (n = 24) or 3 (n=1) in contact with the
 442 anterior chinshields; temporals 1+2 (n = 105), 2+2 (n = 1), 1+1 (n = 1); dorsal scales
 443 rows 19, reducing to 17 rows after midbody (n=74), 18/19/17 (n=8), 18/17/17 (n=7),
 444 with some specimens showing variations in the rows of dorsal scales, usually due to
 445 fusions.

446

447 **Color pattern.** In life, *Erythrolamprus carajasensis* exhibits a brown or gray color on
 448 the head, body, and tail; ventral region of head, body, and tail cream, orange, or red,
 449 with black bands (Fig. 6A). In preserved specimens, head dorsum gray, dark gray or
 450 brown; parietals with pale inner edges (white, light gray or cream), forming V- or Y-
 451 shaped light mark, sometimes reaching frontal and supraocular regions; supralabial,
 452 infralabial and rostral predominantly cream; irregular brown or black spots between
 453 supralabials and infralabials; gular region cream or yellowish with irregular black spots.
 454 Dorsal body gray, dark gray or brown, with dark brown or black crossbands, 3-4 scales
 455 wide dorsally, narrowing laterally (Figs. 3C and 6A) or narrow crossbands with black-
 456 edges scales alternating with light interspaces, formed by scales with white edges (Fig.
 457 3A); blotches irregular or faded, dark pigmentation restricted to dorsal scales edges;
 458 light dorsolateral stripe, cream to white, along fifth and sixth scale rows or extending to
 459 half of seventh rows, more distinct at midbody, reaching tail. Ventral body cream with
 460 black bands, sometimes extending medially, often paired or fused, especially anteriorly.
 461 Tail venter cream with small black dots or spots near the cloacal shield and anterior
 462 subcaudals (Fig. 3A). Juveniles with lighter dorsal background (light brown or light
 463 gray), with more pronounced dark margins, visible dorsolateral stripes (may lack white
 464 pigmentation); ventral surface of the body white background with numerous black
 465 bands, often paired and occasionally fused (Figs. 3C and 6A).

466



Figure 6. General view of **A** juvenile of *Erythrolamprus carajasensis* from Canaã dos Carajás, Pará, Brazil (Photo: Marina Meireles) and **B** *E. almadensis* from Águas de Santa Bárbara, São Paulo, Brazil (Photo: Giordano Rossi).

467

468 **Hemipenial morphology** (n = 11) (Fig. 4A). Hemipenis reaching 9th subcaudal; slightly
 469 bilobed, noncapitate and noncaliculate, with smooth apical disks on the distal surface of
 470 lobes. Hemipenial body covered by numerous spinules. Lobes covered by spinules in
 471 lateral region, on asulcate and sulcate face. On the asulcate face, proximal region with
 472 inflated areas on each side, ornamented with elongated spines arranged in 7–9 rows that

473 decrease as they approach the lobes; nude region at the lower region of the lobes,
474 immediately under the rows of slightly enlarged spinules; and medial region
475 ornamented with a row of elongated spines. Spermatic sulcus bifurcate at mid-body of
476 hemipenial body, centrifugal branches reaching center of apical disks. Intrasulcal region
477 with homogeneously distributed spinules. Basal sulcus spermaticus with inflated area
478 ornamented with elongated spines.

479

480 **Skull osteology** (n = 7) (Fig. 5A–D). Premaxilla triangular in frontal view, with
481 ascending and maxillary processes approximately equal in length; maxillary process not
482 reaching anterior portion of maxilla; ascending process with pointed or narrow apical
483 portion in frontal view, not reaching nasals; vomerine processes short, approaching
484 vomers but remaining distinctly separate. Septomaxillary slightly separated; slight
485 contact with frontals posteriorly, nasal posterior processes posteromedially, and vomers
486 ventrally. Nasals in contact medially; anterior processes coniform and lateral dorsal
487 lamina ranging from wide to narrow; posterior process slightly contacting midventral
488 region of frontals, and dorsomedial region of septomaxillary. Vomers slightly separated,
489 mesoventral portion globular and posteromedial laminae vertical with large exochoanal
490 fenestra. Prefrontals dorsally contact frontals, not reaching maxilla ventrally; posterior
491 region forming anterior orbit margins; anterior process triangular in lateral view; large
492 lacrimal foramen visible in ventral region. Frontals medially united with straight suture,
493 with anteromedial region V-shaped; anterior and posterior margins convex;
494 posterolateral margins concave in dorsal view; forming anterodorsal orbital margin;
495 posterior contact with parietal; ventral edges of vertical laminae approaching but not in
496 contact of frontal, forming deep groove surrounding dorsal projection of
497 parabasisphenoid. Parietal rounded in dorsal view, contacting the postfrontals
498 anterolaterally, prootic and parabasisphenoid ventrally; two oblique dorsolateral crests
499 extending at level of region of contact with postfrontal process to region of contact with
500 supraoccipital; dorsolateral crests without contact. Postfrontals long, narrow and curved,
501 not reaching maxilla, forming posterolateral orbital margin. Supraoccipital wider than
502 long, contacting prootics laterally and otooccipitals posteriorly; two oblique
503 posterolateral ridges, one median posterior ridge. Otooccipitals contacting prootic
504 anterolaterally, supratemporal dorsolaterally, and basioccipital ventrally; ventrally
505 separated, with posterior oblique crests of supraoccipital extending across otooccipitals;
506 forming posterior margin of *fenestra ovalis* at prootic suture. Prootics with 4–5
507 foramina near parabasisphenoid contact (generally one large, one medium and two or
508 three small); surface irregular, dorsally overlain by supratemporal, contacting
509 parabasisphenoid complex anteroventrally and basioccipital complex posteroventrally;
510 forming anterior margin of *fenestra ovalis* at otooccipitals suture. Basioccipital
511 pentagonal, contacting parabasisphenoid complex anteriorly. Parabasisphenoid nearly
512 pentagonal; anterior portion exceeding choanal process of palatine; posterior portion
513 with two small anterolateral and two posterolateral foramina. Maxillae elongated,
514 slightly arched toward premaxilla, extending posterior to level of postfrontals and
515 forming ventral orbital margin; ventral surface of maxilla with 19–22 prediastemal teeth
516 and two enlarged, ungrooved postdiastemal teeth; teeth curved, increasing in size
517 posteriorly, with small diastema; palatine process typically between eleventh and
518 thirteenth tooth, approaching but not contacting maxillary process of palatine. Palatines
519 slender and elongated; 14–16 uniformly sized curved teeth; maxillary process
520 posterolaterally directed, between 5th–8th tooth; choanal process long, nearly

521 rectangular in ventral view, medially curved, level of 8th–11th tooth; posterior end
522 flattened, toothless, contacting pterygoid. Ectopterygoids flattened, maxillary process
523 bifurcated into pointed anteromedial process and quadrangular anterolateral process,
524 approaching but not contacting posterior portion of maxilla; posterior process elongated,
525 ventrally contacting dorsolateral pterygoid. Pterygoids elongate; 25–31 slightly curved
526 teeth; articulation with ectopterygoid between 15th–20th tooth; anterior portion slender
527 to to ~10th tooth, widening posteriorly, tapering posterolaterally between last tooth and
528 rounded posterior end; dorsal surface with longitudinal median ridge posterior to
529 ectopterygoid contact. Supratemporal arched, elongated and laminar, overlapping dorsal
530 portion of prootic, with posterior end freely surpassing posterior edge of otooccipital.
531 Quadrate elongated, straight or obliquely oriented, dorsal portion flattened, wider than
532 the ventral; anterior cephalic edge pronounced; short medial process directed toward
533 columellar, not contacting it. Dentaries elongated, anteriorly curved; 28–30 slightly
534 curved teeth; mental foramen near 14th–15th tooth; branch at 18th–19th tooth into
535 slender dorsal and broader ventral processes; dorsal process branching again at 21st–
536 23rd tooth into short medial process and a longer tooth-bearing dorsal process; contacts
537 splenial medially, compound bone posteriorly, and anterodorsally tip of angular with the
538 tip of medial process. Splenial elongated, triangular, tapering anteriorly and reaching
539 14th–16th dentary tooth; anterior mylohyoid foramen near posterior articulation with
540 angular; posterior edge contacting anterior edge angular. Angular elongated, triangular,
541 and tapered posteriorly, exceeding posterior edge of dentary dorsal process; overlapped
542 by anteroventral portion of compound bone dorsally; posterior mylohyoid foramen near
543 splenial posterior border. Compound bones elongated, tapering anteriorly, fitting
544 between the dorsal and ventral processes of the dentary; prearticular crest prominent,
545 distinctly higher than the surangular crest; retroarticular process medially directed;
546 mandibular foramen oriented laterally.

547

548 **Geographic distribution.** *Erythrolamprus carajasensis* occurs in the Amazon, being
549 restricted to the south by the Amazon River and to the west by Marajó Island (Fig. 7). In
550 Brazil, it is present in the states of Pará, Mato Grosso, Amazonas and Rondônia.

551

552 **Comments.** We observed diagnostic inconsistencies in the original description of
553 *Erythrolamprus carajasensis*. Cunha et al. (1985) did not mention the presence of a
554 light parietal mark, which we observed in the holotype, most paratypes and additional
555 examined specimens. Similarly, the presence of a single apical pit on the dorsal scales
556 was not reported. Variation in the 19/18/17 dorsal scale rows formula occurs due to
557 different row reduction patterns, observed in 1.5% of the analyzed specimens, with most
558 individuals exhibiting 19 dorsal scale rows at midbody. Moreover, the holotype was
559 erroneously listed as a paratype.

560

561

562 ***Erythrolamprus almadensis* (Wagler, 1824)**

563

564 *Natrix almada* Wagler 1824: 30. Type locality: Almada, Bahia, Brazil (Fig. 3B).

565 *Natrix almadensis* Wagler 1824: pl. X, Fig. 3.

566 *Natrix bahiensis* Wagler 1824: 27 (*Incertae sedis*).

567 *Coronella almadensis* — Fitzinger 1826: 895.

- 568 *Liophis almadensis* — Wagler 1830: 188; Boettger 1885: 228; Vanzolini 1986: 12;
 569 Wallach et al. 2014: 388.
 570 *Liophis conirostris* Günther 1858: 46. Type locality: Brazil and Bahia.
 571 *Liophis Wagleri* — Jan 1859: 274.
 572 *Liophis (Lygophis) ygraecum* Peters 1882: 129. Type locality: Vila Guaratinqueta, São
 573 Paulo, Brazil.
 574 *Aporophis conirostris* — Cope 1885: 184.
 575 *Trigonocephalus scolecomorphus* Bacqué 1906: 116. Type locality: Asunción,
 576 Paraguay.
 577 *Leimadophis almadensis* — Serié 1921: 152; Peters and Orejas-Miranda 1970; Jauch
 578 1979; Hoogmoed and Gruber 1983: 331.
 579 *Leimadophis almada* — Vanzolini 1947: 286.
 580 *Dromicus alinadensis* — Cordeiro and Hoge 1974: 262 (*in error*).
 581 *Dromicus almadensis* — Cordeiro and Hoge 1974: 269; Vanzolini 1981: XVIII.
 582 *Erythrolamprus almadensis* — Grazziotin et al. 2012; Nogueira et al. 2019.

583
 584 **Lectotype:** Juvenile, ZSM 2688/0, collected by Spix in “Almada, Bahia, Brazil”.
 585 Hoogmoed and Gruber (1983) designated the lectotype, and Vanzolini (1981) restricted
 586 the type locality to Castelo Novo, municipality of Ilhéus, state of Bahia, Brazil
 587 (14°39'S, 39°10'W) (Fig. 3B).
 588

589 **Paralectotype:** Adult male, ZSM 2747/0, collected by Spix in Brazil and designated by
 590 Hoogmoed and Gruber (1983).
 591

592 **Diagnosis.** *Erythrolamprus almadensis* is distinguished from all its congeners by the
 593 unique combination of the following characters: (1) 19 rows of dorsal scales, reducing
 594 to 17 rows after the midbody; (2) single preocular; (3) ventrals 145–170; (4) subcaudals
 595 54–78; (5) SVL 123–505 mm in females and 138–428 in males; (6) CL 35–148 mm in
 596 females and 38–123 in males; (7) single apical pit; (8) dorsal region of the head with a
 597 light mark formed by the inner edges of the parietals; (9) light dorsolateral stripes,
 598 extending from the anterior region to the tail, between scale rows 5 and 6; (10) cream
 599 belly in preserved material, red in life, with black bands; (11) absence of spines in the
 600 median region of the asulcate face of the hemipenis; (12) well-developed articular and
 601 surangular crests, with adductor fossa dorsally directed; and (13) supratemporal straight
 602 in dorsal view.
 603

604 **Comparisons:** *Erythrolamprus almadensis* differs from the species that have 19/19/17
 605 dorsal scale rows rows as follows: from *E. carajasensis* by developed surangular crest
 606 (vs. reduced surangular crest), and straight supratemporal in dorsal view (vs. arched
 607 supratemporal in dorsal view); from *E. atraventer* by gray dorsal coloration, cream
 608 belly with black bands and the presence of an apical pit (vs. green dorsal coloration,
 609 black belly and absence of apical pit); from *E. festae* by having a single preocular (vs. 2
 610 preoculars); from *E. taeniurus* by the presence of a light dorsolateral stripe (vs. black
 611 lateral stripes bordered by yellow stripes); from *E. viridis* by gray dorsal coloration and
 612 belly with black bands (vs. uniformly green or green back with black bands and
 613 uniformly white belly); and from *E. maryellenae* by the presence of one apical pit (vs.
 614 the absence of the apical pit). Differs from *E. aenigma*, *E. albertguentheri* (Grazziotin,
 615 Zaher, Murphy, Scrocchi, Benavides, Zhang & Bonatto, 2012), *E. ceii*, *E. poecilogyrus*

616 and *E. typhlus* by having 19 dorsal scale rows with reduction in the midbody to 17 scale
 617 rows (vs. 19 dorsal scale rows with reduction in the midbody to 15 scale rows); from *E.*
 618 *andinus*, *E. oligolepis* and *E. aesculapii* by having 19 dorsal scale rows in the midbody
 619 (vs. 15 dorsal scale rows in the midbody); and from *E. breviceps*, *E. cobella*, *E.*
 620 *dorsocorallinus*, *E. frenatus*, *E. jaegeri*, *E. macrosomus*, *E. miliaris*, *E. mossoroensis*, *E.*
 621 *pygmaeus*, *E. reginae*, *E. rochai*, *E. taeniogaster*, *E. trebbauui*, and *E. semiaureus* by
 622 having 19 dorsal scale rows in the midbody (vs. 17 dorsal scale rows in the midbody).

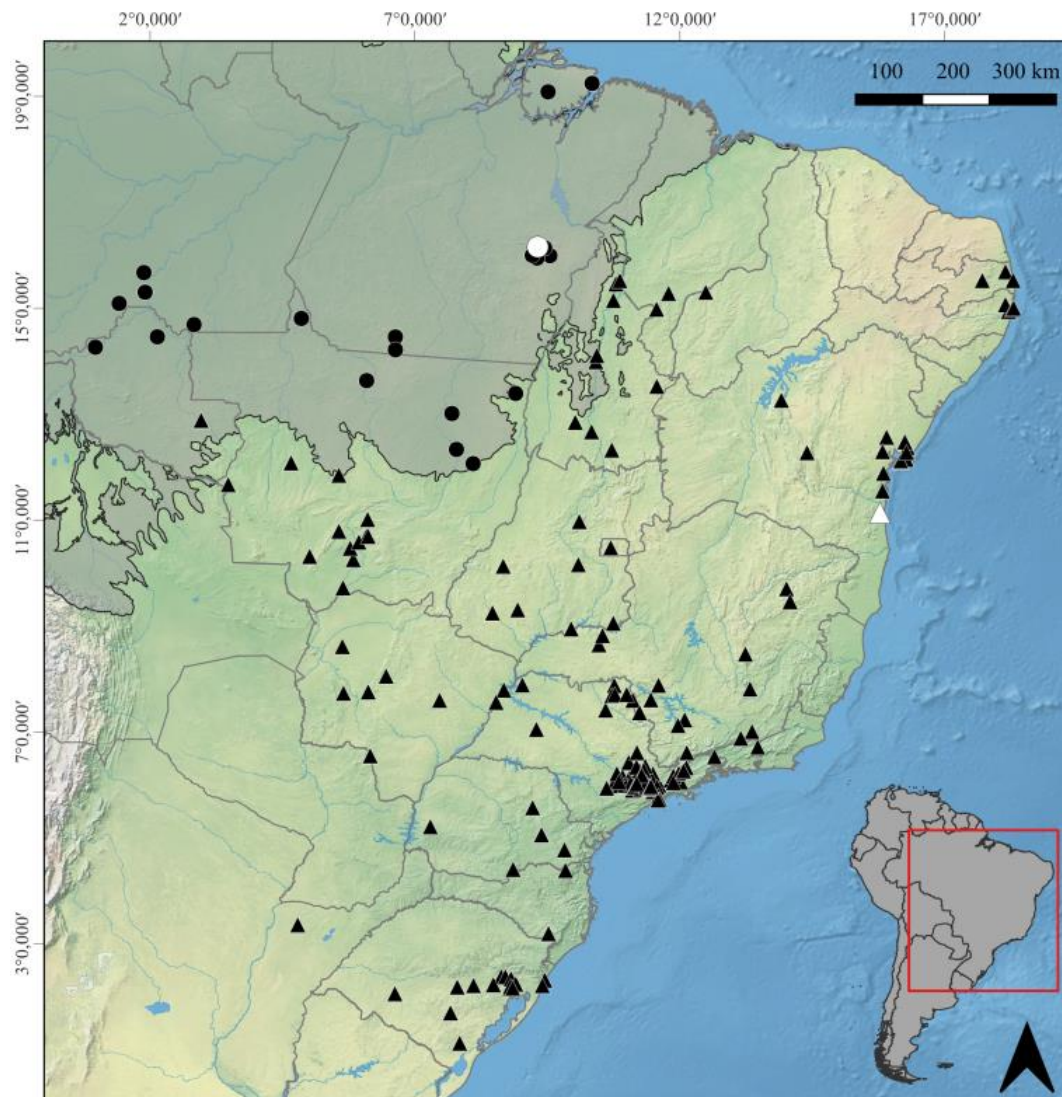
623

624 **Morphometric and meristic variation** (n = 378). Snout-vent length 123–505 mm in
 625 females (341.02±84; n = 213), 138–428 mm in males (309±61.3; n = 167); caudal
 626 length 35–148 mm in females (99.8±24.4; n = 198), 38–123 mm in males (93.2±19.8; n
 627 = 149); head length 10.9–21.2 mm (16.9±1.9; n = 57), height 3.4–7.7 mm (5.86±0.9; n
 628 = 55), and width 4.7–9.6 mm (7.5±1.1; n = 55); diameter of ocular orbit 2.1–3.5 mm
 629 (2.98±0.2; n = 56); distance between the orbit and rostral shield 2.8–6.06 mm (5.02±0.5;
 630 n = 58); rostral triangle, 0.8–1.6 mm high (1.2±0.1; n = 56), 1.95–3.6 mm wide
 631 (2.9±0.3; n = 57); two internals, 0.8–1.6 mm long (1.3±0.1; n = 57), 1.1–2.1 mm wide
 632 (1.6±0.2; n = 56); prefrontals 1.1–2.2 mm long (1.7±0.2; n = 52), 1.5–2.8 mm wide
 633 (2.3±0.2; n = 52); pentagonal frontal, 3.7–5.3 mm long (4.7±0.3; n = 52), 1.9–3.5 mm
 634 wide (2.65±0.3; n = 52); two parietals, 2.3–4.4 mm long (3.6±0.4; n = 58), 2.6–4.1 mm
 635 wide (3.5±0.3; n = 58); loreal 0.6–1.4 mm long (1.03±0.1; n = 56), 0.9–1.6 mm high
 636 (1.3±0.1; n = 56); anterior chinshields 2.2–4.9 mm long (3.6±0.5; n = 55); posterior
 637 chinshields 2.5–4.7 mm long (3.7±0.4; n = 55); ventrals 145–170 in females (155±4.06;
 638 n = 210), 140–166 in males (155± 3.8; n = 168); subcaudals 54–78 in females (64±3.6;
 639 n = 198), 57–76 in males (64±3.5; n = 150); supralabials 8/8 (n = 315), 7/8 (n = 28), 8/9
 640 (n = 1), 4th and 5th in contact with the orbit; infralabials 10/10 (n = 245), 9/10 (n = 86),
 641 9/9 (n = 1), 4 (n = 71) or 5 (n = 191) in contact with the anterior chinshields; temporal
 642 1+2 (n = 53), 2+2 (n = 2), 1+1 (n = 2), 1+3 (n = 1); dorsal scales rows 19, reducing to
 643 17 rows after midbody (n=323), 18/19/17 (n=20), 19/18/17 (n=10), with some
 644 specimens showing variations in the rows of dorsal scales, usually due to fusions.

645

646 **Color pattern.** In life, *Erythrolamprus almadensis* exhibits a brown or gray color on
 647 the dorsal surface of the head, body, and tail; ventral region of head cream, body, and
 648 tail cream, yellowish, orange, or red with black bands (Fig. 6B). In preserved
 649 specimens, dorsum of head gray, dark gray to brown; parietals with inner edges (white,
 650 light gray or cream), forming a light V- or Y-shaped mark, occasionally extending to
 651 frontal and supraocular; supralabial, infralabial and rostral mainly cream; irregular
 652 brown or black spots between the supralabials and infralabials; ventral region cream or
 653 yellowish with irregular black spots on the gulars. Dorsal body gray, dark gray or
 654 brown, with dark brown or black crossbands, 3-4 scales wide at widest portion, at apex
 655 of back, and becoming narrower on sides of body (Figs. 3B and 6B); or narrow
 656 crossbands with black-edged scales alternating with light interspaces, formed by scales
 657 with white edges (Fig. 3D); remaining blotches without defined shape, disappearing in
 658 midbody, with only dark pigmentation at dorsal edges; light dorsolateral stripe, light
 659 brown to white along body, located between the fifth and sixth scale rows, or occupying
 660 half of fifth, and whole sixth, present in anterior region, but more evident in median
 661 region, extending to tail. Ventral region of the body cream, with black bands at lateral
 662 ends of ventrals, reaching middle of scale, in pairs, which may unite, or alternately,
 663 present mainly in anterior portion. Ventral surface of tail cream, with dots or spots near

664 cloacal and first subcaudals (Figs. 3B and 3D). Juveniles with lighter dorsal
 665 background, with light brown or light gray dorsum of head, body and tail, and more
 666 pigmented spots, with a more pronounced color pattern; parietal light spot often extends
 667 to frontal and supraocular areas; ventral region of body with white background with
 668 numerous black bands, often in pairs or joined together (Fig. 3B).
 669



670
 671 **Figure 7.** Geographic distribution of *Erythrolamprus carajasensis* (triangle) and *E. almadensis* (circle).
 672 White symbols represent type localities.
 673

674 **Hemipenial morphology** (n = 19) (Fig. 4B). Hemipenis reaching 10th subcaudal;
 675 slightly bilobed, noncapitate and noncaliculate, with smooth apical disks on the distal
 676 surface of the lobes. Hemipenial body covered by numerous spinules. Lobes covered by
 677 spinules in lateral region, on asulcate and sulcate face. On the asulcate face, proximal
 678 region with inflated areas on each side, ornamented with elongated spines arranged in
 679 7–9 rows that decrease as they approach the lobes; nude region at the lower region of
 680 the lobes, immediately under the rows of slightly enlarged spinules; and medial region
 681 ornamented with a row of elongated spines. Spermatic sulcus bifurcates at mid-body of
 682 hemipenial, with divergent branches in centrifugal position, reaching center of apical

683 disks. Intrasulcal region with homogeneously distributed spinules. Basal region of
684 sulcus spermaticus with inflated area ornamented with elongated spines.

685

686 **Skull osteology** (n = 16) (Fig. 5E–H). Premaxilla triangular in frontal view, with
687 ascending and maxillary processes of approximately equal length; maxillary process not
688 reaching anterior portion of maxilla; ascending process with apical portion ranging from
689 pointed to blunt in frontal view, not reaching nasals; short vomerine processes,
690 approaching vomers but remaining distinctly separate. Septomaxillary slightly
691 separated, in slight contact with frontals posteriorly, posterior processes of nasals
692 posteromedially, and vomers ventrally. Nasals in contact medially; anterior processes
693 coniform and wide lateral dorsal lamina; posterior process slightly contacts midventral
694 region of the frontals, and the posterior part of septomaxillary dorsomedial region.
695 Vomers slightly separated, with globular mesoventral portion and vertical
696 posteromedial laminae with large exochoanal fenestra; palatine process ranging from
697 blunt or tapered. Prefrontals in contact with frontals dorsally, not reaching maxilla
698 ventrally; posterior region forming anterior margins of orbits; anterior process and
699 lateral footprocess tapered in lateral view; in frontal view, large lacrimal foramen
700 visible in ventral region. Frontals medially united with straight suture, with
701 anteromedial region V-shaped; anterior and posterior margins convex and posterior
702 lateral margins concave in dorsal view; forming anterodorsal margin of orbits;
703 posteriorly contacting parietal; ventral edges of vertical laminae of frontals approaching
704 but not in contact, forming deep groove that dorsally and laterally surrounds dorsal
705 projection of parabasisphenoid. Parietal rounded in dorsal view, contacting postfrontals
706 anterolaterally, prootic and parabasisphenoid ventrally, with two oblique dorsolateral
707 ridges extending at level of region of contact with postfrontal process to region of
708 contact with supraoccipital; dorsolateral crests without contact. Postfrontals long,
709 narrow and curved, not reaching maxilla, forming posterolateral margin of orbit.
710 Supraoccipital wider than long, in contact with prootics laterally, and otooccipitals
711 posteriorly; with two oblique ridges oriented posterolaterally and one medial oriented
712 posteriorly. Otooccipitals in contact with prootic anterolaterally, supratemporal
713 dorsolaterally, and with basioccipital ventrally; ventrally separated, with posterior
714 oblique ridges of supraoccipitals extending across otooccipitals; forms posterior part of
715 *fenestra ovalis* at its suture with prootic. Prootics with multiple foramina near region of
716 contact with parabasisphenoid; generally, one large, one medium and two small
717 foramina; irregular surface, dorsally largely overlain by supratemporal, in contact with
718 parabasisphenoid complex anteroventrally and basioccipital complex posteroventrally;
719 forming anterior margin of *fenestra ovalis* at suture with otooccipitals. Basioccipital
720 pentagonal, in contact with parabasisphenoid complex anteriorly. Parabasisphenoid
721 nearly pentagonal; anterior portion exceeds choanal process of palatine; posterior
722 portion with two small anterolateral and two posterolateral foramina. Maxillae
723 elongated and slightly arched toward premaxilla, extending to posterior level of
724 postfrontals and forming ventral margin of orbit; ventral surface of maxilla with
725 prediastemal teeth ranging from 19–22 enlarged and ungrooved postdiastemal teeth;
726 teeth curved, increasing in size posteriorly, with small diastema; palatine process is
727 usually situated between 11th–15th tooth, approaching but not in contact with the
728 maxillary process of the palatine. Palatines slender and elongated; ventral surface with
729 sixteen curved, uniformly sized teeth; maxillary process directed posterolaterally,
730 usually situated between the sixth to eighth tooth; choanal process long, nearly

731 rectangular in ventral view, curved, and directed medially, situated at level of 9th–11th
732 tooth; posterior end flattened and toothless, in contact with pterygoid. Ectopterygoids
733 flattened, with maxillary process bifurcated into pointed anteromedial process and
734 nearly quadrangular anterolateral process, approaching but not contacting posterior
735 portion of maxilla; posterior process elongated, ventrally contacting dorsal surface of
736 lateromedial region of pterygoid. Pterygoids elongate; ventral surface 27–30 slightly
737 curved teeth; usually articulates with ectopterygoid at level of 15th–22th tooth; anterior
738 portion slender usually to level of 12 tooth, widening posteriorly up to level of the last
739 tooth and tapering posterolaterally between last tooth and rounded posterior end; dorsal
740 surface with median longitudinal ridge that extends from point posterior to contact zone
741 with ectopterygoid to posterior end. Supratemporal straight and laminar; overlapping
742 much of dorsal portion of prootic, with posterior end freely surpassing posterior edge of
743 otooccipital. Quadrate elongated and robust, obliquely oriented; dorsal portion flattened
744 and distinctly wider than ventral portion; short process situated medially, toward
745 columellar shaft but remaining distinctly separate; ventral portion contacts glenoid
746 cavity of retroarticular process of compound bone. Dentaries elongated, medially curved
747 anteriorly; dorsal surface with twenty-eight to thirty slightly curved teeth; mental
748 foramen situated near level of the 13th–14th tooth; dentary branching at about level of
749 the nineteenth tooth, into a longer slender tooth-bearing dorsal process, and a shorter
750 and broader ventral process; dorsal process branching again at the level between the 21-
751 23 tooth into very short medial process and much longer tooth-bearing dorsal process;
752 contacting splenial medially, compound bone posteriorly, and anterodorsally tip of
753 angular with the tip of medial process. Splenial elongated, triangular, tapering anteriorly
754 and reaching level between the 15th–16th tooth of dentary; anterior mylohyoid foramen
755 near posterior articulation with angular; posterior edge in contact with anterior edge
756 angular. Angular elongated, triangular, and narrow posteriorly; in contact with
757 anteroventral portion of composite bone dorsally; posterior mylohyoid foramen near
758 posterior border of splenial. Compound bone elongated, tapering anteriorly, fitting
759 between dorsal and ventromedial processes of dentary; prearticular crest prominent,
760 distinctly higher than surangular crest; retroarticular process stout, medially directed,
761 mandibular foramen oriented dorsolaterally.

762

763 **Geographic distribution.** *Erythrolamprus almadensis* is distributed in Argentina,
764 Bolivia, Brazil, Paraguay and Uruguay. In Brazil, it occurs widely throughout the
765 Cerrado, Pampas, Pantanal and Atlantic Forest, with marginal records in the Caatinga
766 (Fig. 7).

767

768 **Comments.** Wagler (1824) described *Erythrolamprus almadensis* as *Natrix almada*
769 and, in the illustration legend, as *N. almadensis*, based on a specimen collected by Spix
770 in the “outskirts of Almada, near the city of Bahia” (Fig. 7). Fitzinger (1826), the first
771 reviewer of the species, gave precedence to the epithet *almadensis*. Vanzolini (1947)
772 argued that, according to the International Code of Zoological Nomenclature (Amaral
773 1937), the epithet *almada* should be adopted due to page precedence; however, this rule
774 applies only in the absence of a prior review. We follow Peters and Orejas-Miranda
775 (1970) and Hoogmoed and Gruber (1983) in maintaining the use of *almadensis*, based
776 on the first reviewer rule as established in Article 24.2 of the International Code of
777 Zoological Nomenclature (1999), and due to its widespread usage in the literature (e.g.,
778 Wagler 1830; Boettger 1885; Boulenger 1886; Serié 1916, 1921; Amaral 1926, 1929;

779 Cordeiro and Hoge 1974; Vanzolini 1981, 1986; Dixon 1980, 1991; Graziotin et al.
780 2012; Wallach et al. 2014).

781
782 Additionally, Vanzolini (1947) identified Almada as corresponding to Castelo
783 Novo, in the municipality of Ilhéus, state of Bahia, Brazil. According to the itinerary of
784 Spix and Martius (1828), the Almada Farm was located approximately seven leagues
785 (ca. 33 km) northwest of the village of São Jorge dos Ilhéus, currently the municipality
786 of Ilhéus. This farm neighbored the Castel-Novo farm and was the last settlement
787 upstream along the Itaípe River, now known as the Almada River. Furthermore, Lagoa
788 de Almada—currently called Lagoa Encantada—lies about one and a half leagues (ca. 7
789 km) northeast of Almada. Upon revisiting the travel records of Spix and Martius,
790 Vanzolini (1981) reaffirmed this interpretation, which has been followed by subsequent
791 authors (Franzen and Glaw 2007; Oliveira et al. 2022). However, Nogueira et al. (2019)
792 listed the type locality of *E. almadensis* as “Almada, Itajuípe, state of Bahia, Brazil”.
793 Although the Almada River passes both Castelo Novo (Ilhéus) and Itajuípe—separated
794 by approximately 29 km—Castelo Novo lies only about 32 km from Ilhéus and 7 km
795 from Lagoa Encantada, while Itajuípe is located roughly 63 km and 37 km away from
796 those locations, respectively. Based on the Spix and Martius itinerary, we consider
797 Castelo Novo, municipality of Ilhéus, state of Bahia, Brazil, to be the type locality of *E.*
798 *almadensis*.

799

800 Discussion

801

802 Our integrative analysis combining molecular, morphological, and geographic data
803 provides robust support for the recognition of *Erythrolamprus carajasensis* as a species
804 distinct from *E. almadensis*. Although both taxa exhibit overlapping external
805 morphologies and hemipenial characteristics, key differences in skull morphology,
806 congruent with mitochondrial phylogeny and geographic segregation, clearly delineate
807 these lineages as independently evolving units.

808

809 Our phylogenetic analysis based on the concatenated mitochondrial fragments
810 (12S + 16S; 1,167 bp) recovered the monophyly of Xenodontini and recover *Lygophis*
811 as sister to clade comprising *Xenodon* and *Erythrolamprus*, in agreement with previous
812 studies (Zaher et al. 2009, 2019; Vidal et al. 2010; Graziotin et al. 2012; Jowers et al.
813 2013; Pyron et al. 2013; Figueroa et al. 2016; Torres-Carvajal and Hinojosa 2020;
814 Entiauspe-Neto et al. 2021; Moraes et al. 2021; Serrano et al. 2024). However, our
815 results highlight significant taxonomic incongruities within *Erythrolamprus*,
816 particularly its paraphyletic recovery due to the position of *E. sagittifer*, which grouped
817 with *Lygophis* species with maximal posterior probability. This finding, corroborated by
818 earlier observations (e.g., Cacciali et al. 2019), reinforces the need for a critical
819 reassessment of *E. sagittifer*'s generic placement and further integration of
820 morphological and molecular data in this lineage. Dixon and Thomas (1982)
821 highlighted morphological similarities between *E. sagittifer* and the long-tailed species
822 of the *Lygophis lineatus* group (*Ly. lineatus*, *Ly. dilepis*, *Ly. flavifrenatus*, *Ly. paucidens*
823 and *Ly. meridionalis*) (*sensu* Michaud and Dixon 1987). Conversely, the monophyly of
824 *Erythrolamprus* has been previously supported with high phylogenetic support based on
825 molecular data (Zaher et al. 2009, 2019; Vidal et al. 2010; Graziotin et al. 2012; Pyron
826 et al. 2013; Figueroa et al. 2016; Murphy et al. 2019; Torres-Carvajal and Hinojosa

827 2020; Serrano et al. 2024), although these studies did not include *E. sagittifer* and
828 instead recovered the same clade of species that we recovered with strong support.

829

830 Within *Erythrolamprus*, our analysis recovered two major clades (A and B),
831 although clade B showed relatively weak support. Clade A comprises *E. atraventer*, *E.*
832 *jaegeri*, *E. almadensis*, and *E. carajasensis*, with the last two forming a well-supported
833 group subdivided into two subclades (A1 and A2). This clade as previously reported
834 (Grazziotin et al. 2012; Pyron et al. 2013; Figueroa et al. 2016; Murphy et al. 2019;
835 Zaher et al. 2019; Torres-Carvajal and Hinojosa 2020; Entiauspe-Neto et al. 2021;
836 Serrano et al. 2024) as a sister to all other remaining species in the genus (Pyron et al.
837 2013; Zaher et al. 2019; Torres-Carvajal and Hinojosa 2020). In contrast to previous
838 hypotheses (Torres-Carvajal and Hinojosa 2020; Entiauspe-Neto et al. 2021), we
839 recovered *E. almadensis* as a monophyletic clade. We recovered *E. carajasensis* nested
840 within a northern Amazonian subclade (A1), distinct from the southern and eastern
841 populations of *E. almadensis* (subclade A2). Although *E. carajasensis* and *E.*
842 *almadensis* showed only shallow genetic divergence (16S p-distances ranging from
843 0.002–0.018), this variation is consistent with interspecific thresholds previously used in
844 the genus (e.g., Torres-Carvajal and Hinojosa 2024), and notably, with the pattern of
845 geographical structuring observed between subclades.

846

847 Although external morphology alone was insufficient for diagnosing the
848 recovered lineages, multivariate analyses based on morphometric data (PCA and
849 DAPC) were successful in discriminating between subclades A1 and A2, particularly
850 when sexes were analyzed separately. Females and males from subclades A1 and A2
851 showed statistically significant differences in several morphometric traits, with the
852 DAPC assigning over 91% of specimens to their correct groups. These patterns suggest
853 some degree of morphometric differentiation, possibly reflecting adaptation to different
854 environmental conditions or historical isolation. Nonetheless, overlap in several traits
855 emphasizes the cryptic nature of these lineages.

856

857 Most compelling are the cranial morphological differences, particularly the
858 slenderer cranial elements observed in *E. carajasensis* from the Carajás region, such as
859 shape of the quadrate and supratemporal, configuration of the surangular crest and
860 mandibular foramen. These features contrast with the more robust skulls of *E.*
861 *almadensis*, especially from the Atlantic Forest and Cerrado regions, and are consistent
862 with previous findings that cranial shape in snakes can be influenced by ecological
863 factors including habitat use and diet (Klaczko et al. 2016; Santos et al. 2017;
864 Papežíková et al. 2024). While the ecological drivers of cranial variation in these taxa
865 remain unclear, the observed divergence underscores the evolutionary independence of
866 these lineages.

867

868 The hemipenial morphology was largely conserved across both species,
869 including organ shape, ornamentation, and the arrangement of spinules, with only minor
870 variation observed within and between clades. This conservatism limits the diagnostic
871 utility of reproductive characters for distinguishing *E. carajasensis* and *E. almadensis*, a
872 pattern also observed in other xenodontine snakes (e.g., Entiauspe-Neto et al. 2021).

873

874 Geographically, our results redefine the distribution of *E. almadensis* as limited
875 to extra-Amazonian populations primarily in eastern and southern Brazil, with
876 confirmed records from Bahia, Tocantins, Minas Gerais, São Paulo, Santa Catarina, and
877 Rio Grande do Sul. In contrast, *E. carajasensis* is now recognized as occupying the
878 Amazonian populations previously attributed to *E. almadensis*, including areas in Pará,
879 Amazonas, and northern Mato Grosso. The Amazon–Tocantins interfluvium emerges as a
880 likely barrier separating the two species, as seen in other Amazonian taxa (e.g., Naka et
881 al. 2012), possibly reflecting historical vicariance or ecological constraints on dispersal.

882
883 These findings have broader implications for understanding the diversity and
884 biogeography of *Erythrolamprus* in South America. The high level of cryptic diversity
885 revealed here may reflect past vicariant events or ecological shifts associated with major
886 biogeographic barriers such as the Amazon River or the "dry diagonal"
887 (Caatinga/Cerrado). Finally, our results underscore the value of combining molecular
888 phylogenetics, external and internal morphology, and robust statistical analyses to
889 resolve taxonomic uncertainties in morphologically conservative snake lineages.

890 **References**

- 891
- 892 Amaral A (1926) South American snakes in the collection of the United States National
893 Museum. *Proceedings of the United States National Museum* 67 (2596): 1–30.
894 <https://doi.org/10.5479/si.00963801.2596>
- 895
- 896 Amaral A (1929) Estudos sobre Ophidios Neotrópicos. XVIII Lista remissiva dos
897 ophidios da região Neotrópica. *Memorias do Instituto Butantan* 4: 129–271.
898
- 899 Amaral A (1937) Regras Internacionais de Nomenclatura Zoológica (Tradução para o
900 português). *Memorias do Instituto Butantan* 11: 241–274.
901
- 902 Ascenso AC, Costa JCL, Prudente ALC (2019) Taxonomic revision of the
903 *Erythrolamprus reginae* species group, with description of a new species from
904 Guiana Shield (Serpentes: Xenodontinae). *Zootaxa* 4586 (1): 65–97.
905 <https://doi.org/10.11646/zootaxa.4586.1.3>
- 906
- 907 Bacqué A (1906) Trois *Trigonocéphales* du Paraguay. *Revista del Museo de La Plata*
908 12: 113–119.
909 <https://publicaciones.fcnym.unlp.edu.ar/rmlp/article/view/1234/1327>
- 910
- 911 Boettger O (1885) Liste von Reptilien and Batrachiern aus Paraguay. *Zeitschrift Für*
912 *Naturwissenschaften* 58: 213–248. <https://www.biodiversitylibrary.org/part/69906>
- 913
- 914 Boulenger G (1886) A synopsis of the reptiles and batrachians of the Province Rio
915 Grande do Sul. *Annals and Magazine of Natural History* 18: 423–445.
916 <https://biostor.org/reference/49287>
- 917
- 918 Cacciali P, Buongermini E, Köhler G (2019) Barcoding Analysis of Paraguayan
919 Squamata. *Diversity* 11 (9): 152. <https://doi.org/10.3390/d11090152>
- 920
- 921 Chan KO, Grismer LL (2022) GroupStruct: An R Package for Allometric Size
922 Correction. *Zootaxa* 5124 (4): 471–482. <https://doi.org/10.11646/zootaxa.5124.4.4>
- 923
- 924 Cope ED (1885) Twelfth Contribution to the Herpetology of Tropical America.
925 *Proceedings of the American Philosophical Society* 22 (118): 167–194.
926 <http://www.jstor.org/stable/982675>
- 927
- 928 Cordeiro CL, Hoge AR (1974) Contribuição ao conhecimento das serpentes do Estado
929 de Pernambuco. *Memórias do Instituto Butantan* 37: 261–290.
930 <http://bibliotecadigital.butantan.gov.br/colecao/memorias-do-instituto-butantan>
- 931
- 932 Cundall D, Irish F (2008) The snake skull. In: *Biology of the Reptilia* 20, Morphology.
933 Society for the Study of Amphibians and Reptiles, Ithaca, 349–692.
934
- 935 Cunha OR, Nascimento FP, Ávila-Pires TCS (1985) Os répteis da área de Carajás, Pará,
936 Brasil (Testudines e Squamata). I. *Publicações Avulsas do Museu Paraense*
937 *Emílio Goeldi* 40: 9–92. <https://repositorio.museu-goeldi.br/handle/mgoeldi/564>

- 938
 939 Dixon JR, Markezich AL (1992) Taxonomy and geographic-variation of *Liophis*
 940 *poecilogyrus* (Wied) from South-America (Serpentes: Colubridae). Texas Journal
 941 of Science 44: 131–166.
 942
- 943 Dixon JR (1980) The Neotropical colubrid snake genus *Liophis*: the generic concept.
 944 Milwaukee Public Museum. Contributions in Biology and Geology 31: 1–40.
 945
- 946 Dixon JR (1983a). Systematics of *Liophis reginae* and *L. williamsi* (Serpentes,
 947 Colubridae), with a description of a new species. Carnegie Museum of Natural
 948 History 52: 113–138. <https://doi.org/10.5962/p.215198>
 949
- 950 Dixon JR (1983b) The *Liophis cobella* group of the neotropical colubrid snake genus
 951 *Liophis*. Journal of Herpetology 17: 149–165. <https://doi.org/10.2307/1563456>
 952
- 953 Dixon JR (1989) A key and checklist to the neotropical snake genus *Liophis* with
 954 country list and maps. Smithsonian Herpetological Information Service 79: 1–28.
 955 <https://doi.org/10.5479/si.23317515.79.1>
 956
- 957 Dixon JR (1991) Geographic variation and taxonomy of *Liophis almadensis* (Wagler)
 958 (Serpentes: Colubridae), and description of a new species of *Liophis* from
 959 Argentina and Bolivia. The Texas Journal of Science 43: 225–236.
 960
- 961 Dixon JR, Thomas RA (1982) The status of the Argentine colubrid snakes *Liophis*
 962 *sagittifer* and *L. trifasciatus*. Herpetologica: 389–395.
 963
- 964 Dixon JR, Thomas RA (1985) A new species of South American water snake (genus
 965 *Liophis*) from southeastern Brazil. Herpetologica: 259–262.
 966 <http://www.jstor.org/stable/3892271>
 967
- 968 Dowling HG (1951) A proposed standard system of counting ventrals in snakes. British
 969 Journal of Herpetology 1(5): 97–99.
 970
- 971 Entiauspe-Neto OM, Abegg AD, Koch C, Nuñez LP, Azevedo WS, Moraes LJCL,
 972 Tiutenko A, Bialves TS, Loebmann D (2021) A new species of *Erythrolamprus*
 973 (Serpentes: Dipsadidae: Xenodontini) from the savannas of northern South
 974 America. Salamandra 57: 196–218. <https://repositorio.inpa.gov.br/handle/1/37770>
 975
- 976 Figueroa A, McKelvy AD, Grismer LL, Bell CD, Lailvaux SP (2016) A species-level
 977 phylogeny of extant snakes with description of a new colubrid subfamily and
 978 genus. PLOS ONE 11, e0161070. <https://doi.org/10.1371/journal.pone.0161070>
 979
- 980 Fitzinger LJ (1826) Kritische Bemerkungen über J. Wagler’s Schlangenwerk. Isis von
 981 Oken 19: 881–909. <https://www.biodiversitylibrary.org/bibliography/13271>
 982
- 983 Franco FL (2012) A coleção herpetológica do Instituto Butantan: da sua origem ao
 984 incêndio ocorrido em 15 de maio de 2010. Herpetologia Brasileira 1: 22–31.

- 985
 986 Franzen M, Glaw F (2007) Type catalogue of reptiles in the Zoologische
 987 Staatssammlung München. Spixiana 30(2): 201–274.
 988
 989 Grazziotin FG, Zaher H, Murphy RW, Scrocchi G, Benavides MA, Zhang YP, Bonatto
 990 SL (2012) Molecular phylogeny of the New World Dipsadidae (Serpentes
 991 Colubriodea): a reappraisal. Cladistics 1:1–23. [https://doi.org/10.1111/j.1096-](https://doi.org/10.1111/j.1096-0031.2012.00393.x)
 992 [0031.2012.00393.x](https://doi.org/10.1111/j.1096-0031.2012.00393.x)
 993
 994 Günther A (1858) Catalogue of colubrine snakes in the collection of the British
 995 Museum. Printed by order of the Trustees 4. 318 pp.
 996 <https://doi.org/10.5962/bhl.title.13272>
 997
 998 Hoogmoed M, Gruber U (1983) Spix and Wagler type specimens of reptiles and
 999 amphibians in the Natural History Museum in Munich (Germany) and Leiden (The
 1000 Netherlands). Spixiana Supplement 9: 319–415.
 1001
 1002 Hudson AA, Curcio FF, Sousa BM, Marques OAV (2021) The South American false
 1003 coral snake *Erythrolamprus aesculapii* (Serpentes: Dipsadidae) as a possible
 1004 mimic of *Micrurus averyi* (Serpentes: Elapidae) in Central Amazonia.
 1005 Phyllomedusa 20: 93–98. <http://dx.doi.org/10.11606/issn.2316-9079.v20i1p93-98>
 1006
 1007 Jan G (1859) Spix' Serpentes brasiliensis. 272–275. In: Erichson, W. F. 45. Archiv für
 1008 Naturgeschichte. <https://www.biodiversitylibrary.org/page/13716144>
 1009
 1010 Jan G, Sordelli F (1866) Iconographie générale des ophidiens II. Chez l'auteur.
 1011 <https://doi.org/10.5962/bhl.title.45246>
 1012
 1013 Jauch H (1979) Brasilianische Schlangen im Terrarium. Herpetofauna 1: 6–9.
 1014
 1015 Jombart T, Collins C (2015) A tutorial for discriminant analysis of principal
 1016 components (DAPC) using adegenet 2.0.0.
 1017
 1018 Jowers MJ, Caut S, Garcia-Mударra JL, Alasaad S, Ineich I (2013) Molecular
 1019 Phylogenetics of the Possibly Extinct Martinique Ground Snake. Herpetologica
 1020 69: 227–236. <https://doi.org/10.1655/HERPETOLOGICA-D-12-00085>
 1021
 1022 Katoh K, Rozewicki J, Kazunori DY (2019) MAFFT online service: Multiple sequence
 1023 alignment, interactive sequence choice and visualization. Briefngs in
 1024 Bioinformatics 20(4): 1160–1166. <https://doi.org/10.1093/bib/bbx108>
 1025
 1026 Kearse M, Moir R, Wilson A, Stones-Havas S, Cheung M, Sturrock S, Buxton S,
 1027 Cooper A, Markowitz S, Duran C, Thierer T, Ashton B, Meintjes P, Drummond A
 1028 (2012) Geneious Basic: An integrated and extendable desktop software platform
 1029 for the organization and analysis of sequence data. Bioinformatics 28(12): 1647–
 1030 1649. <https://doi.org/10.1093/bioinformatics/bts199>
 1031

- 1032 Klaczko J, Sherratt E, Setz EZF (2016) Are Diet Preferences Associated to Skulls Shape
 1033 Diversification in Xenodontine Snakes? PLoS ONE 11(2): e0148375.
 1034 <https://doi.org/10.1371/journal.pone.0148375>
 1035
- 1036 Kumar A (2010) A tragic loss: fire at Instituto Butantan, Brazil. Toxicon 1528–1529.
 1037 <https://doi.org/10.1016/j.toxicon.2010.07.002>
 1038
- 1039 Kumar S, Stecher G, Tamura K (2016) MEGA7: molecular evolutionary genetics
 1040 analysis version 7.0 for bigger datasets. Molecular biology and evolution 33(7):
 1041 1870–1874. <https://doi.org/10.1093/molbev/msw054>
 1042
- 1043 Michaud EJ, Dixon JR (1987) Taxonomic revision of the *Liophis lineatus* complex
 1044 (Reptilia: Colubridae) of Central and South America. Milwaukee Public Museum
 1045 Contribution in Biology and Geology 71:1–26.
 1046
- 1047 Miller MA, Pfeiffer W, Schwartz T (2010) Creating the CIPRES Science Gateway for
 1048 inference of large phylogenetic trees. Gateway Computing Environments
 1049 Workshop (GCE): 1–8. <https://doi.org/10.1109/GCE.2010.5676129>
 1050
- 1051 Minh BQ, Schmidt HA, Chernomor O, Schrempf D, Woodhams MD, Haeseler A,
 1052 Lanfear R (2020) IQ-TREE 2: new models and efficient methods for phylogenetic
 1053 inference in the genomic era. Molecular Biology and Evolution 37: 1530–1534.
 1054 <https://doi.org/10.1093/molbev/msaa015>
 1055
- 1056 Moraes LJCL, Entiauspe-Neto OM, de Fraga R, Fernandes IY, Werneck FP (2021)
 1057 Systematics of the rare Amazonian genus *Eutrachelophis* (Serpentes: Dipsadidae),
 1058 with an emended diagnosis for *Eutrachelophis papilio*. Zoologischer Anzeiger
 1059 295: 191–204. <https://doi.org/https://doi.org/10.1016/j.jcz.2021.10.003>
 1060
- 1061 Murphy JC, Braswell AL, Charles SP, Auguste RJ, Rivas GA, Borzée A, Lehtinen RM,
 1062 Jowers MJ (2019) A new species of *Erythrolamprus* from the oceanic island of
 1063 Tobago (Squamata, Dipsadidae). ZooKeys 2019: 131–157.
 1064 <https://doi.org/10.3897/zookeys.817.30811>
 1065
- 1066 Myers CW (1986) An Enigmatic New Snake from the Peruvian Andes, with Notes on
 1067 the Xenodontini (Colubridae: Xenodontinae). American Museum of Natural
 1068 History 2853: 1–12. <http://hdl.handle.net/2246/5200>
 1069
- 1070 Naka LN, Bechtoldt CL, Henriques LMP, Brumfield RT (2012) The role of physical
 1071 barriers in the location of avian suture zones in the Guiana Shield, northern
 1072 Amazonia. The American Naturalist 179(4): E115–E132.
 1073 <https://doi.org/10.1086/664627>
 1074
- 1075 Nogueira CC, Argôlo AJS, Arzamendia V, Azevedo JA, Barbo FE, Bérnils RS,
 1076 Bolochio BE, Borges-Martins M, Brasil-Godinho M, Braz H, Buononato MA,
 1077 Cisneros-Heredia DF, Colli GR, Costa HC, Franco FL, Giraud A, Gonzalez RC,
 1078 Guedes T, Hoogmoed MS, Marques OAV, Montingelli GG, Passos P, Prudente
 1079 ALC, Rivas GA, Sanchez PM, Serrano FC, Silva NJ, Strüssmann C, Vieira-

- 1080 Alencar JPS, Zaher H, Sawaya RJ, Martins M (2019) Atlas of Brazilian Snakes:
 1081 Verified Point-Locality Maps to Mitigate the Wallacean Shortfall in a
 1082 Megadiverse Snake Fauna. *South American Journal of Herpetology* 14: S1–S274.
 1083 <https://doi.org/10.2994/SAJH-D-19-00120.1>
 1084
- 1085 Oliveira EF, Costa HC, São-Pedro VA, Marques R, Santana DJ, Colli GR, Mesquita
 1086 DO, Costa GC (2022) On the type locality of *Ameivula ocellifera* (Spix, 1825)
 1087 (Squamata, Teiidae), with a neotype designation. *Zoosystema* 44(19): 475–491.
 1088 <https://doi.org/10.5252/zoosystema2022v44a19>
 1089
- 1090 Papežíková S, Ivanov M, Papežík P, Javorčík A, Mebert K, Jablonski D (2024)
 1091 Comparing morphology and cranial osteology in two divergent clades of dice
 1092 snakes from continental Europe (Squamata: Natricidae: *Natrix tessellata*).
 1093 *Vertebrate Zoology* 3(74): 511–31. <https://doi.org/10.3897/vz.74.e123824>
 1094
- 1095 Peters JA (1964) *Dictionary of Herpetology*. Hafner Publishing, New York 488 p.
 1096
- 1097 Peters JA, Orejas-Miranda B (1970) *Catalogue of the Neotropical Squamata 1. Snakes*.
 1098 Smithsonian Institution Press, Washington, 347 pp.
 1099 <https://doi.org/https://doi.org/10.5962/bhl.title.46653>
 1100
- 1101 Peters WCH (1882) Den Namen der Batrachiergattung Hylonomus em Hyloscirtus zu
 1102 ändern und legte zwei neue Arten von Schlangen, *Microsoma notatum* e *Liophis*
 1103 *ygraecum*. *Sitzungsber. Gesellschaft Naturforschender Freunde zu Berlin* 8: 127–
 1104 129. <https://www.biodiversitylibrary.org/bibliography/7922>
 1105
- 1106 Pyron RA, Burbrink FT, Wiens JJ (2013) A phylogeny and revised classification of
 1107 Squamata, including 4161 species of lizards and snakes. *BMC Evolutionary*
 1108 *Biology* 13: 93–146. <https://doi.org/10.1186/1471-2148-13-93>
 1109
- 1110 QGIS Development Team 2022. *QGIS: Quantum GIS Geographic Information System*.
 1111 Open Source Geospatial Foundation Project. Version 3.24.3.
 1112
- 1113 Rambaut A, Drummond AJ, Xie D, Baele G, Suchard MA (2018) Posterior
 1114 summarisation in Bayesian phylogenetics using Tracer 1.7. *Systematic Biology*
 1115 67(5): 901–904. <https://doi.org/10.1093/sysbio/syy032>
 1116
- 1117 Santos MM, Silva FM, Hingst-Zaher E, Machado FA, Zaher HE, Prudente ALC (2017)
 1118 Cranial adaptations for feeding on snails in species of *Sibynomorphus*
 1119 (Dipsadidae: Dipsadinae). *Zoology* 120: 24–30.
 1120 <https://doi.org/10.1016/j.zool.2016.09.003>
 1121
- 1122 Serrano FC, Pontes- Gonzales M, Sawaya RJ, Alencar LRV, Nogueira CC, Grazziotin
 1123 FG (2024) There and back again: when and how the world's richest snake family
 1124 (Dipsadidae) dispersed and speciated across the Neotropical region. *Journal of*
 1125 *Biogeography*: 1–16. <https://doi.org/10.1111/jbi.14790>
 1126

- 1127 Serié P (1916) Sobre tres supuestos nuevos *Trigonocephalus* del Paraguay. *Physis*
1128 2:171–174. <https://www.biodiversitylibrary.org/item/110337>
1129
- 1130 Serié P (1921) Catálogo de los ofidios argentinos. *Anales de la Sociedad Científica*
1131 Argentina 92:145–175. <https://biostor.org/reference/161134>
1132
- 1133 Silva FM, Prudente ALC, Machado FA, Santos MM, Zaher H, Hingst-Zaher E
1134 (2018) Aquatic adaptations in a Neotropical coral snake: A study of
1135 morphological convergence. *Journal of Zoological Systematics and Evolutionary*
1136 *Research* 56: 382–394. <https://doi.org/10.1111/jzs.12202>
1137
- 1138 Silveira AL, Prudente ALC, Argôlo AJS, Abrahão CR, Nogueira CC, Barbo FE, Costa
1139 GC, Pontes GMF, Colli GR, Zaher H, Borges-Martins M, Martins MRC, Oliveira
1140 ME, Passos PGH, Bérnils RS, Sawaya RJ, Cechin CTZ, Guedes da Costa, TB
1141 (2021) *Erythrolamprus carajasensis*. The IUCN Red List of Threatened Species
1142 2021: e.T15179213A123739731. [https://dx.doi.org/10.2305/IUCN.UK.2021-](https://dx.doi.org/10.2305/IUCN.UK.2021-3.RLTS.T15179213A123739731)
1143 [3.RLTS.T15179213A123739731](https://dx.doi.org/10.2305/IUCN.UK.2021-3.RLTS.T15179213A123739731)
1144
- 1145 Spix JB, Martius CFP (1828) Reise em Brasilien. *Munique*: IJ Lentner.
1146 <https://doi.org/10.5962/bhl.title.16406>
1147
- 1148 Thorpe RS (1975) Quantitative handling of characters useful in snake systematics with
1149 particular reference to intraspecific variation in the Ringed Snake *Natrix natrix*
1150 (L.). *Biological Journal of the Linnean Society* 7: 27–43.
1151 <https://doi.org/10.1111/j.1095-8312.1975.tb00732.x>
1152
- 1153 Torres-Carvajal O, Hinojosa KC (2020) Hidden diversity in two widespread snake
1154 species (Serpentes: Xenodontini: *Erythrolamprus*) from South America.
1155 *Molecular Phylogenetics and Evolution* 146: 1–8.
1156 <https://doi.org/10.1016/j.ympev.2020.106772>
1157
- 1158 Torres-Carvajal O, Hinojosa KC, Paucar DA (2024) A New Species of *Erythrolamprus*
1159 (Serpentes: Dipsadidae) from the Andes of Ecuador. *Journal of Herpetology*,
1160 58(2):1–11. <https://doi.org/10.1670/2237051>
1161
- 1162 Uetz P, Freed P, Aguilar R, Hošek J (2024) The Reptile Database. ([http://www.reptile-](http://www.reptile-database.org/)
1163 [database.org/](http://www.reptile-database.org/)) [Accessed on 10.09.2024].
1164
- 1165 Vaidya G, Lohman DJ, Meier R (2011) SequenceMatrix: Concatenation software for
1166 the fast assembly of multi-gene datasets with character set and codon information.
1167 *Cladistics* 27(2): 171–180. <https://doi.org/10.1111/j.1096-0031.2010.00329.x>
1168
- 1169 Vanzolini PE (1947) Nota nomenclatural sobre *Leimadophis almada* (Wagler, 1824) (= *Leimadophis almadensis* Auct.). *Papéis Avulsos de Zoologia* 8: 285–286.
1170 <https://www.biodiversitylibrary.org/page/55786534>
1171
1172
- 1173 Vanzolini PE (1981) The scientific and political contexts of the Bavarian Expedition to
1174 Brasil. *Herpetology of Brazil*.

- 1175
 1176 Vanzolini PE (1986) Addenda and corrigenda to the Catalogue of the Neotropical
 1177 Squamata. Smithsonian Herpetological Information Service Washington 70: 1–26.
 1178
- 1179 Vidal N, Dewynter M, Gower DJ (2010) Dissecting the major American snake
 1180 radiation: A molecular phylogeny of the Dipsadidae Bonaparte (Serpentes,
 1181 Caenophidia). *Comptes Rendus Biologies* 333: 48–55.
 1182 <https://doi.org/10.1016/j.crvi.2009.11.003>
 1183
- 1184 Wagler J (1824) *Serpentum Brasiliensium species novae, ou histoire naturelle des*
 1185 *espèces nouvelles de serpens*. In: Jean de Spix, *Animalia nova sive species novae*.
 1186 Monaco, Typis Franc. Seraph. Hübschmanni vii 75 pp.
 1187 <https://doi.org/10.5962/bhl.title.4269>
 1188
- 1189 Wagler J (1830) *Natürliches System der Amphibien, mit vorangehender Classification*
 1190 *der Säugthiere und Vogel*. J. G. Cotta, München, Stuttgart und Tübingen, 167 pp.
 1191 <https://doi.org/10.5962/bhl.title.108661>
 1192
- 1193 Wallach V, Williams KL, Boundy J (2014) *Snakes of the world: a catalogue of living*
 1194 *and extinct species*. CRC press 1227 pp.
 1195
- 1196 Warrell DA, Theakston RDG, Wüster W (2010) Destruction of the collection of reptiles
 1197 and arthropods at Butantan Institute: a view from the United Kingdom. *The*
 1198 *Journal of Venomous Animals and Toxins including Tropical Diseases* 16: 534–
 1199 536. <https://doi.org/10.1590/S1678-91992010000400003>
 1200
- 1201 Wickham H (2016) *ggplot2—Elegant Graphics for Data Analysis*. 2^a ed. Springer, 260
 1202 pp.
 1203
- 1204 Zaher H (1999) Hemipenial morphology of the South American xenodontinae snakes,
 1205 with a proposal for a monophyletic Xenodontinae and a reappraisal of colubroid
 1206 hemipenes. *Bulletin of the American Museum of Natural History* 240: 1–172.
 1207 <http://hdl.handle.net/2246/1646>
 1208
- 1209 Zaher H, Grazziotin FG, Cadle JE, Murphy RW, Moura-Leite CJ, Bonatto SL (2009)
 1210 Molecular phylogeny of advanced snakes (Serpentes, Caenophidia) with an
 1211 emphasis on South American Xenodontines: a revised classification and
 1212 descriptions of new taxa. *Papéis Avulsos de Zoologia* 49: 115–153.
 1213 <https://doi.org/10.1590/S0031-10492009001100001>
 1214
- 1215 Zaher H, Murphy RW, Arredondo JC, Graboski R, Machado-Filho PR, Mahlow K,
 1216 Montingelli GG, Quadros AB, Orlov NL, Wilkinson M, Zhang Y-P, Grazziotin
 1217 FG (2019) Large-scale molecular phylogeny, morphology, divergence-time
 1218 estimation, and the fossil record of advanced caenophidian snakes (Squamata:
 1219 Serpentes). *PLoS One* 14: e0216148.
 1220 <https://doi.org/10.1371/journal.pone.0216148>
 1221

- 1222 Zaher H, Mohabey DM, Grazziotin FG, Wilson Mantilla JA (2023) The skull of
1223 *Sanajeh indicus*, a Cretaceous snake with an upper temporal bar, and the origin of
1224 ophidian wide-gaped feeding. *Zoological Journal of the Linnean Society* 197(3):
1225 656-697. <https://doi.org/10.1093/zoolinnea/zlac001>
1226
- 1227 Zaher H, Prudente ALC (2003) Hemipenis of *Siphlophis* (Serpentes, Xenodontinae) and
1228 techniques of hemipenial preparation in snakes: a response to Dowling.
1229 *Herpetological Review* 34: 302–307.